HHS Public Access

Author manuscript

Nat Cell Biol. Author manuscript; available in PMC 2016 May 18.

Published in final edited form as:

Nat Cell Biol. 2015 December ; 17(12): 1546–1555. doi:10.1038/ncb3266.

IRE1α is an endogenous substrate of endoplasmic reticulum-associated degradation

Shengyi Sun[1,17], **Guojun Shi**[2,3,17], **Haibo Sha**[2], **Yewei Ji**[2], **Xuemei Han**[4], **Xin Shu**[2], **Hongming Ma**[5], **Takamasa Inoue**[6], **Beixue Gao**[7], **Hana Kim**[2], **Pengcheng Bu**[8], **Robert D. Guber**[2], **Xiling Shen**[8], **Ann-Hwee Lee**[9], **Takao Iwawaki**[10], **Adrienne W. Paton**[11], **James C. Paton**[11], **Deyu Fang**[7], **Billy Tsai**[6], **John R. Yates III**[4], **Haoquan Wu**[5], **Sander Kersten**[12], **Qiaoming Long**[13,18], **Gerald E. Duhamel**[14], **Kenneth W. Simpson**[15], and **Ling Qi**[1,2,16,18]

[1]Graduate Program in Biochemistry, Molecular and Cell Biology, Cornell University, Ithaca, NY 14853 [2]Division of Nutritional Sciences, Cornell University, Ithaca, NY 14853 [3]Shanghai Institute of Endocrine and Metabolic Diseases, Ruijin Hospital, Shanghai Jiaotong University School of Medicine, Shanghai 200025, China [4]Department of Chemical Physiology, The Scripps Research Institute, La Jolla, CA 92037 [5]Department of Biomedical Sciences, Paul L. Foster School of Medicine, Texas Tech University Health Sciences Center, El Paso, TX 79905 [6]Department of Cell and Developmental Biology, University of Michigan Medical School, Ann Arbor, MI 48105 [7]Department of Pathology, Northwestern University, Chicago, IL 60611 [8]Department of Electrical and Computer Engineering, and Department of Biomedical Engineering, Cornell University, Ithaca, NY 14853 [9]Department of Pathology and Laboratory Medicine, Weill Cornell Medical College, New York, NY 10021, USA [10]Education and Research Support Center, Gunma University Graduate School of Medicine, 3-39-22 Showa-machi, Maebashi, Gunma 371-8511, Japan [11]Research Centre for Infectious Diseases, School of Molecular and Biomedical Science, University of Adelaide, Adelaide, SA 5005, Australia [12]Nutrition Metabolism and Genomics group, Wageningen University, Wageningen, The Netherlands [13]Laboratory Animal Research Center, Medical College of Soochow University, Suzhou 215006, Jiangsu, China [14]Department of Biomedical Sciences, College of Veterinary Medicine, Cornell University, Ithaca, NY 14853 [15]Department of Clinical Science, College of Veterinary Medicine, Cornell University, Ithaca, NY

[18]Correspondence should be addressed to: ; Email: lq35@cornell.edu (L. Qi); ; Email: qmlong@suda.edu.cn (Q. Long)
[17]These authors contribute equally

The authors declare no competing financial interests.

AUTHOR CONTRIBUTION

S.S. designed and performed most in vivo experiments; G.S. designed and performed most in vitro experiments; X.H. and J.R.Y. performed the proteomic analysis; S.S., P.B. and X.S. performed the organoid culture; Y.J. assisted some in vivo experiments; H.S. generated various enterocyte cell lines; H.S., S.S. and X.S. performed some in vitro analyses; H.K. and R.D.G. repeated some in vitro experiments; B.G. and D.F. generated inducible Hrd1 knockout mice; H.M. and H.W. generated SEL1L-knockout HEK293T cells; T.Inoue and B.T. performed limited proteolysis analysis; T.I., A.L., A.W.P., J.C.P. and Q.L. provided key reagents; S.K. performed microarray analyses; G.E.D. performed histological examination of the tissue; K.W.S. performed FISH and designed the experiments; L.Q. conceived the project and designed the experiments. L.Q. and S.S. wrote the manuscript, S.S. and G.S. wrote the methods and figure legends, and everybody edited and approved the manuscript.

MICROARRAY DATASET ACCESSION NUMBER: **GSE70563**.

14853 [16]Department of Immunology, School of Medicine, Jiangsu University, Zhenjiang, Jiangsu 212013, China

Abstract

Endoplasmic reticulum (ER)-associated degradation (ERAD) represents a principle quality control mechanism to clear misfolded proteins in the ER; however its physiological significance and the nature of endogenous ERAD substrates remain largely unexplored. Here we discover that IRE1α, the sensor of unfolded protein response (UPR), is a bona fide substrate of the Sel1L-Hrd1 ERAD complex. ERAD-mediated IRE1α degradation occurs under basal conditions in a BiP-dependent manner, requires both intramembrane hydrophilic residues of IRE1α and lectin protein OS9, and is attenuated by ER stress. ERAD deficiency causes IRE1α protein stabilization, accumulation and mild activation both in vitro and in vivo. Although enterocyte-specific Sel1L-knockout mice (*Sel1L*$^{\Delta IEC}$) are viable and appear normal, they are highly susceptible to experimental colitis and inflammation-associated dysbiosis, in an IRE1α-dependent but CHOP-independent manner. Hence, Sel1L-Hrd1 ERAD serves a distinct, essential function in restraint of IRE1α signaling in vivo by managing its protein turnover.

Keywords

ER; Sel1L; Hrd1; ERAD; UPR; intestinal epithelium; inflammation; colitis

INTRODUCTION

The endoplasmic reticulum (ER) is the principle site for the folding and quality-control (QC) of proteins destined for the secretory pathway. Both physiological and pathological processes affect the workload in the ER. The imbalance of ER homeostasis often results in the aggregation of misfolded proteins in different cellular compartments, which are hallmarks of human diseases including cystic fibrosis, α1-antitrypsin deficiency and aging. Misfolded proteins in the ER are mainly recognized and targeted for proteasomal degradation by the ER-associated degradation (ERAD) machinery[1,2]. Identification of artificial proteins and disease-related mutant proteins as ERAD substrates has brought important insights into ERAD biology and the pathogenesis of ERAD-associated diseases, respectively[1]. However, our understanding of the importance of ERAD function under physiological settings is very limited because of the lack of animal models and physiologically relevant endogenous substrates.

Among several known mammalian ERAD complexes, the Sel1L-Hrd1 complex forms a principle ERAD machinery, responsible for the recognition and retrotranslocation of a subset of misfolded proteins in the ER for cytosolic proteasomal degradation[3–9]. Using inducible and adipocyte-specific Sel1L-deficient mouse and cell models, we recently provided in vivo evidence demonstrating that Sel1L is a key component of mammalian Hrd1 ERAD machinery and that Sel1L-Hrd1 complex plays a critical role in the maintenance of ER homeostasis[10,11]. Loss of Sel1L leads to a profound reduction of Hrd1 protein level with a concomitant accumulation of a lectin protein OS9, pointing to an indispensable role of

Sel1L in Hrd1 function[10,11]. Intriguingly, loss of Sel1L in the pancreatic acinar cells causes exocrine pancreatic insufficiency associated with significant cell atrophy[10]. By contrast, Sel1L deficiency in adipocytes has no obvious effect on cell death, but rather causes intracellular retention of lipoprotein lipase in the ER, leading to postprandial hypertriglyceridemia[11]. These intriguing findings point to a cell type-specific effect of Sel1L-Hrd1 ERAD as well as the significance of specific substrates in mediating the ERAD effect in vivo.

Accumulation of misfolded proteins in the ER activates unfolded protein response (UPR). IRE1α, the most conserved UPR sensor, is a type-1 transmembrane ER-resident protein with bifunctional cytosolic kinase and RNase domains. IRE1α is associated with the ER chaperone BiP (or GRP78) under basal conditions[12]. Upon sensing of misfolded proteins in the ER, IRE1α dissociates from BiP, undergoes dimer-/oligomerization and trans-autophosphorylation via its kinase domain, which activates its RNase activity towards *Xbp1* mRNA and leads to the generation of an active transcription factor XBP1s[13–15]. XBP1s transcriptionally regulates the expression of many ER chaperone, lipogenic and ERAD genes[16]. Genetic studies have revealed that XBP1 is a risk factor for inflammatory bowel disease (IBD)[17]. In intestinal epithelium-specific *Xbp1*-deficient mice, IRE1α protein is hyperactivated, which promotes the development of IBD in part via the activation of JNK[17,18].

Here we report the discovery of IRE1α as a bona fide endogenous substrate of the Sel1L-Hrd1 ERAD complex both in vitro and in vivo, and elucidate underlying molecular mechanisms under both basal and stress conditions. Using intestinal epithelial-specific *Sel1L*-deficient mice, we further demonstrate the pathological significance of ERAD-mediated IRE1α degradation in experimental colitis. Our data illustrates how the actions of ER QC systems, ERAD and UPR, are coordinated to cultivate a dynamic nature of ER homeostasis.

RESULTS

IRE1α is an endogenous ERAD substrate in vitro

Acute loss of Sel1L in *Sel1Lf/f;ERCre+* mouse embryonic fibroblasts (MEFs) treated with tamoxifen analog 4-OHT (*Sel1L*^{IKO}) leads to ERAD defect[10] with dilated ER, when compared to that of *Sel1Lf/f;ERCre+* MEFs treated with vehicle (WT) (Fig. 1a). In a search for endogenous Sel1L-Hrd1 substrates in the ER, we performed quantitative LC-MS/MS analysis of purified microsomal/ER fractions from *Sel1L*^{IKO} and WT MEFs (Supplementary Fig. 1a), which identified a total of 3,220 proteins (Supplementary Table 1). Among many proteins overrepresented in *Sel1L*^{IKO} MEFs were the lectin protein OS9, a known substrate of Sel1L-Hrd1 ERAD[10,11], and surprisingly, the UPR sensor IRE1α (Supplementary Fig. 1b). Western blot analysis of total cell lysates confirmed the accumulation of OS9 and IRE1α proteins in *Sel1L*^{IKO} MEFs (Supplementary Fig. 1c). The elevated protein levels of IRE1α and OS9 were not due to increased transcription as the abundance of *Ire1a* and *Os9* mRNA was actually reduced in *Sel1L*^{IKO} MEFs (Supplementary Fig. 1d). Moreover, IRE1α protein level, but not PERK, was negatively correlated with the levels of Sel1L and Hrd1 (Fig. 1b–c). Excluding a non-specific drug effect, 4-OHT treatment had no effect on IRE1α

protein level in *f/f;ERCre−* MEFs (Fig. 1d). Pointing to a role of Hrd1 in IRE1α protein turnover, IRE1α protein was stabilized and accumulated in Hrd1-deficient MEFs (Fig. 1e–f and Supplementary Fig. 1e).

To determine whether IRE1α ERAD is conserved in humans, we employed the CRISPR/Cas9-mediated knockout of *SEL1L* in human HEK293T cells. Endogenous IRE1α and OS9 proteins were greatly stabilized in *SEL1L*-deficient HEK293T cells, which was not seen for the cytosolic protein BAG6 (Fig. 1g). In both *Hrd1−/−* MEFs and *SEL1L−/−* HEK293T cells, IRE1α protein accumulation was independent of transcriptional upregulation (Supplementary Fig. 1f–g). Moreover, IRE1α protein synthesis rate was comparable between WT and *SEL1L−/−* HEK293T cells as demonstrated by the ^{35}S-labelled methionine/cysteine incorporation assay (Supplementary Fig. 1h). Thus, IRE1α is a substrate of SEL1L-HRD1 ERAD, conserved from mice to humans.

Substrate recognition by Sel1L-Hrd1 ERAD

ERAD proceeds through four tightly coupled steps, substrate selection, retrotranslocation to the cytosol, ubiquitination conjugation, and proteasomal degradation[2]. Hrd1 interacted with IRE1α and prompted IRE1α polyubiquitination via its catalytic RING finger domain in transfected HEK293T cells (Fig. 2a). Sample denaturation prior to IRE1α immunoprecipitation confirmed ubiquitination directly on IRE1α protein (Supplementary Fig. 2a). Consistent with the idea that disruption of the RING finger motif of Hrd1 prolongs the interaction with its substrate[19], IRE1α interacted much stronger with the catalytic inactive Hrd1 compared to WT Hrd1 (Fig. 2a). Overexpression of Hrd1 partially reversed IRE1α accumulation in *Sel1L^{IKO}* MEFs (Fig. 2b and Supplementary Fig. 2b), suggesting that both Sel1L and Hrd1 are indispensable for IRE1α degradation.

We next addressed how Sel1L-Hrd1 ERAD complex identifies IRE1α as a potential ERAD substrate. OS9, a lectin protein, is known to recruit misfolded substrates, both glycosylated and non-glycosylated, to the Sel1L-Hrd1 ERAD complex[20,21]. OS9 interacted strongly with IRE1α (Supplementary Fig. 2c). Deletion of OS9 increased IRE1α protein level and its stability (Fig. 2c–e and Supplementary Fig. 2d–e).

Inspired by the elegant work in yeast[22], we explored the role of intramembrane hydrophilic residues of IRE1α in its degradation. The transmembrane domain of IRE1α contains three hydrophilic amino acids (T446, S450, T451), highly conserved from humans to fish (Fig. 2f). Mutating them to alanine (T446A, S450A and T451A, in short T3A) led to IRE1α protein accumulation and stabilization (Fig. 2g–i). Indeed, the T3A mutation reduced IRE1α ubiquitination and attenuated its interaction with Hrd1 (Fig. 2j), without affecting protein intracellular distribution or stress responsiveness (Supplementary Fig. 2f–g). Thus, both OS9 and intramembrane hydrophilic residues of IRE1α may operate in parallel in ERAD-mediated IRE1α degradation.

The role of ER stress in IRE1α degradation

MG132 treatment significantly increased IRE1α ubiquitination (Fig. 3a), pointing to the involvement of proteasome in IRE1α degradation. Intriguingly, IRE1α ubiquitination was reduced when challenged with pharmacological ER stressor thapsigargin (Fig. 3a and

Supplementary Fig. 2h). The effect of ER stress on IRE1α ubiquitination was persistent even in the presence of MG132 (Fig. 3a), suggesting that ER stress affects IRE1α degradation upstream of protein ubiquitination. Moreover, IRE1α interaction with Hrd1 and endogenous Sel1L was attenuated in response to ER stress (Fig. 3b–c). IRE1α protein increased by nearly 5-fold during ER stress in WT cells whereas only 1.5 fold in *Sel1L*^{IKO} MEFs (Supplementary Fig. 2i), pointing to the contribution of IRE1α protein stabilization to its accumulation during ER stress. Indeed, IRE1α protein was dramatically stabilized under ER stress (Fig. 3d). Hence, ER stress attenuates Sel1L-Hrd1-mediated IRE1α ubiquitination and degradation.

ER stress is triggered by the accumulation of misfolded proteins in the ER, and is known to initiate dimer-/oligomerization of IRE1α. To test whether misfolded proteins may compete with IRE1α for ERAD, we overexpressed a model ERAD substrate α1-antitrypsin variant null^{HongKong} (NHK) in HEK293T cells. Indeed, model substrates interacted strongly with endogenous SEL1L and significantly attenuated the interaction between IRE1α and SEL1L (Fig. 3e). Moreover, ER stress induced dimer-/oligomerization of IRE1α protein as revealed by sucrose density gradient ultracentrifugation followed by non-reducing SDS-PAGE analyses (Fig. 3f) and was associated with increased resistance to trypsin digestion (Fig. 3g), pointing to a conformational change of IRE1α during ER stress. Thus, ER stress increases the level of ERAD substrates in the ER and triggers conformational change of IRE1α, which may attenuate the interaction between IRE1α and the ERAD complex.

The role of Bip in IRE1α degradation

BiP dissociates from IRE1α during ER stress (Fig. 4a)[12]. Given the role of BiP in protein folding and degradation[23], we next explored its role in IRE1α degradation. Cleavage of BiP with the subtilase cytotoxin SubAB[24] abolished the interaction between IRE1α and Sel1L (Fig. 4b), reduced IRE1α ubiquitination (Supplementary Fig. 2j) and importantly, significantly stabilized IRE1α (Fig. 4c). Conversely, ectopic expression of BiP attenuated the accumulation of IRE1α protein during ER stress (Fig. 4d), without affecting its mRNA level (Supplementary Fig. 2k). The effect of BiP overexpression on IRE1α protein level was seen only under ER stress condition (Fig. 4d), consistent with the notion that BiP becomes limited and dissociates from IRE1α during ER stress[12].

We next investigated BiP association and ERAD degradation of a dimerization-incompetent IRE1α mutant[25,26]. Mutation of IRE1α at the residue Asp123 to Pro (D123P) rendered IRE1α largely irresponsive to ER stress as demonstrated by the lack of ER stress-induced IRE1α phosphorylation (Fig. 4e). Unlike WT protein, D123P IRE1α interacted constitutively with endogenous BiP (Fig. 4e) and failed to be stabilized under stress conditions (Fig. 4f). Hence, we conclude that BiP plays a key role in targeting IRE1α for ERAD degradation under basal conditions and that ER stress triggers BiP-IRE1α dissociation and dimer-/oligomerization of IRE1α, leading to IRE1α dissociation from the ERAD complex and protein stabilization.

IRE1α is an endogenous ERAD substrate in vivo

As dysregulated IRE1α signaling in intestinal epithelium has been implicated in the pathogenesis of IBD[17,18], we generated intestinal epithelial cell (IEC)-specific Sel1L-deficient mice (*Sel1L*$^{\Delta IEC}$). *Sel1L*$^{\Delta IEC}$ and *Sel1L*$^{flox/flox}$ (WT) control littermates were born at the expected Mendelian ratios (Supplementary Fig. 3a) and grew at comparable rates for both females and males (Fig. 5a). Both Sel1L and Hrd1 protein levels was significantly reduced in the gut of *Sel1L*$^{\Delta IEC}$ mice (Fig. 5b–c). These mice were deficient for epithelial ERAD function as demonstrated by the accumulation of OS9 protein (Fig. 5b–c).

IRE1α protein level was elevated by over 15-fold in the colonic epithelium of *Sel1L*$^{\Delta IEC}$ mice (Fig. 5b–c), while its mRNA level was not altered (Fig. 5d). The accumulation of both IRE1α and OS9 proteins in the colonic epithelium was confirmed by immunohistochemistry (Fig. 5e and Supplementary Fig. 3b). To argue against developmental defects as a possible cause for IRE1α accumulation in *Sel1L*$^{\Delta IEC}$ mice, acute loss of either Sel1L or Hrd1 caused a significant accumulation of IRE1α protein without affecting its mRNA level (Fig. 5f–i). Further supporting the notion that epithelial IRE1α is an ERAD substrate, IRE1α protein was highly stabilized in primary intestinal crypt organoids from *Sel1L*$^{\Delta IEC}$ mice (Fig. 5j–k). By contrast, ERAD deficiency had no effect on the protein or mRNA levels of IRE1α homolog IRE1β (Supplementary Fig. 3c), despite a ~50% identity in amino acid sequences. Of note, three intramembrane hydrophilic residues were not conserved between IRE1α and IRE1β proteins (Supplementary Fig. 3d).

We next tested whether Sel1L-Hrd1-mediated IRE1α degradation is a general phenomenon. IRE1α protein level was highly elevated in the pancreas of *Sel1L*^{IKO} mice at day 4 and 8 post-tamoxifen injection[10] (Supplementary Fig. 3e) and white adipose tissue of adipocyte-specific *Sel1L*-deficient (AKO or *Sel1L*$^{\Delta adipo}$) mice[11] (Supplementary Fig. 3f). *Ire1a* mRNA level was not affected by *Sel1L* deficiency (Supplementary Fig. 3g and not shown). IRE1α protein was significantly stabilized in *Sel1L*$^{\Delta adipo}$ primary adipocytes (Fig. 5l). Taken together, our data demonstrate that IRE1α is a bona fide endogenous ERAD substrate in vivo.

A regulatory circuit of IRE1α and Sel1L-Hrd1

In both yeast and mammalian cells, IRE1α signaling pathway regulates the expression of ERAD components[15]. We next performed both gain- and loss-of-function studies to determine whether this is true in enterocytes. Overexpression of XBP1s in small intestinal crypt m-IC$_{cl2}$ enterocytes increased the expression of *Sel1L, Hrd1* and *Os9* (Supplementary Fig. 4a). Conversely, knockout of IRE1α or XBP1 in m-IC$_{cl2}$ enterocytes attenuated the expression of ERAD components including *Sel1L, Hrd1* and *Os9* (Supplementary Fig. 4b–c). Thus, our data establish a negative regulatory circuit consisting of IRE1α-XBP1 and the Sel1L-Hrd1 ERAD in enterocytes (Supplementary Fig. 4d).

Restraint of IRE1α signaling by ERAD

In *Sel1L*$^{\Delta IEC}$ enterocytes, IRE1α was hyperphosphorylated and activated as measured by mobility shift of phosphorylated IRE1α protein[27–29] and *Xbp1* mRNA splicing (Fig. 6a–c). Similar observations were obtained in other models with acute or chronic Sel1L deficiency,

including *Sel1L*^{IKO} MEFs (Fig. 6d–e), pancreas (Supplementary Fig. 3e), ileum (Supplementary Fig. 4e) and *Sel1L*$^{\Delta adipo}$ adipose tissue (Supplementary Fig. 4f–g). Without Sel1L, accumulated IRE1α proteins, including phosphorylated IRE1α, did not form NP-40 insoluble aggregates in the epithelium (Fig. 6f) and were highly responsive to ER stress (Fig. 6g–h). Consistently, *Xbp1s* mRNA level was much higher in *Sel1L*-deficient adipocytes when treated with thapsigargin (Fig. 6i). Moreover, crypt organoids isolated from *Sel1L*$^{\Delta IEC}$ mice exhibited elevated JNK phosphorylation in response to TNFα stimulation (Fig. 6j). Similarly, knockdown of Sel1L in enterocytes elevated TNFα-induced JNK phosphorylation (Supplementary Fig. 4h–j) and *Tnfa* expression (Fig. 6k). Therefore, Sel1L-Hrd1 ERAD restrains IRE1α signaling and attenuates IRE1α-associated inflammation, at least in part, via ERAD-mediated IRE1α degradation.

Sensitivity to experimental colitis

To our surprise, the length and gross morphology of the colon of *Sel1L*$^{\Delta IEC}$ mice appeared normal, indistinguishable from those of WT littermates under basal conditions (Fig. 7a and Supplementary Fig. 5a). There was no increase of cell death or signs of spontaneous colitis in the colonic epithelium of *Sel1L*$^{\Delta IEC}$ mice (Fig. 7a–b). Genome-wide microarray analysis of colonic epithelium revealed that inflammation and cell death pathways were not upregulated in *Sel1L*$^{\Delta IEC}$ mice under basal conditions (Supplementary Table 2). In keeping with elevated IRE1α signaling (Fig. 6), top upregulated pathways identified by the microarray were the “protein processing in the ER”, “UPR” and “activation of ER chaperones by IRE1α” (Supplementary Fig. 5b). Genes involved in UPR and ERAD such as *Derlin 3, Pdia6, Trib3*, and *BiP* were among the top genes induced in the epithelium of *Sel1L*$^{\Delta IEC}$ mice when compared to WT littermates (Supplementary Fig. 5c and Table 3).

Treatment with dextran sodium sulfate (DSS) induces epithelial TNFα signaling and triggers epithelial injury and colitis, a widely used model to study disease pathogenesis of IBD[30]. Indeed, colonic epithelia of *Sel1L*$^{\Delta IEC}$ mice exhibited a significant increase of cell death following DSS challenge (Fig. 7c–d and Supplementary Fig. 5d). *Sel1L*$^{\Delta IEC}$ mice developed more severe clinical signs of mucosal inflammation and colitis, including body weight loss (Fig. 7e), gross rectal bleeding and diarrhea (Supplementary Fig. 5e). The majority of *Sel1L*$^{\Delta IEC}$ mice (~90%) succumbed to DSS treatment by day 12 (Fig. 7f). Colon shortening, a typical clinical feature of colonic inflammation, was more pronounced in *Sel1L*$^{\Delta IEC}$ mice (Fig. 7g). Histological examination of the distal colon of *Sel1L*$^{\Delta IEC}$ mice revealed a near complete loss of epithelium and crypts, increased colonic mucosal damage/erosion, massive immune cell infiltration and lymphoid foci formation, and edema (Fig. 7h–i). The difference in colitis sensitivity was not due to variable DSS intake (Supplementary Fig. 5f).

DSS-induced colitis and lethality were prevented by co-administration of broad-spectrum antibiotics in the drinking water (Fig. 7f). FISH analysis of *Eubacteria* demonstrated more severe bacterial invasion of the colonic mucosa of DSS-treated *Sel1L*$^{\Delta IEC}$ mice. Patchy bacterial invasion into the epithelium, thick mats of superficial invasive bacteria associated with diffuse ulceration and intraluminal bacterial proliferation in epithelial cell debris were commonly observed in the *Sel1L*$^{\Delta IEC}$ samples (Supplementary Fig. 5g). Interestingly, although not commonly present in the colon under basal conditions, invasive *E. coli* were

observed on and within colonic mucosa of *Sel1L*$^{\Delta IEC}$ mice (panel 1, Fig. 7j), or associated with dead cells sloughed off the epithelium (panel 2, Fig. 7j). Adherent and invasive *E. coli* has been previously associated with pathogenesis of human Crohn's disease and murine ileitis[31]. Gut microbial composition was expectedly very similar in co-housed WT and *Sel1L*$^{\Delta IEC}$ mice under basal conditions (Supplementary Fig. 5h), with Enterobacteriaceae including the Family of *E. coli* barely detectable in the feces of both cohorts (not shown). Thus, intestinal inflammation may drive *E. coli*-dominated dysbiosis and bacterial invasion as previously reported[32].

In keeping with increased invasive and adherent bacteria in the colonic epithelium of DSS-treated *Sel1L*$^{\Delta IEC}$ mice, activated CD8^{+} T cells were elevated in the spleen and mesenteric lymph nodes (Supplementary Fig. 5i). Inflammatory cytokines that have been linked to endotoxemia and sepsis[33], including macrophage inflammatory protein 2 (MIP2), granulocyte-colony stimulating factor (G-CSF) and platelet-derived growth factor β polypeptide (PDGF-BB), were significantly increased in the circulation of DSS-treated *Sel1L*$^{\Delta IEC}$ mice (Supplementary Fig. 5j). Similar trend was observed for IL-1β, TNFα and IL-6, albeit not statistically significant. These data point to a severe systemic pro-inflammatory response in DSS-treated *Sel1L*$^{\Delta IEC}$ mice. In the aggregate, Sel1L is dispensable for the gross morphology of the colon, but its deficiency sensitizes the animal to experimental colitis and inflammation-induced dysbiosis.

Pathological significance of IRE1α degradation

To determine whether IRE1α accumulation modulates the pathogenesis of experimental colitis, we generated *Sel1L*$^{\Delta IEC}$ mice with only one copy of epithelial *Ire1a* gene (*Sel1L*$^{\Delta IEC}$;*Ire1a*+/−) (Supplementary Fig. 6a–b) and subjected them, together with three other control cohorts, to DSS-induced colitis. *Sel1L*$^{\Delta IEC}$;*Ire1a*+/− mice were less sensitive to DSS-induced colitis, with ameliorated body weight loss and colon shortening when compared to that of DSS-treated *Sel1L*$^{\Delta IEC}$ mice (Fig. 8a–b). Histological assessment revealed attenuated colonic damage in DSS-treated *Sel1L*$^{\Delta IEC}$;*Ire1a*+/− mice compared to that of *Sel1L*$^{\Delta IEC}$ mice (Fig. 8c). IRE1α protein level in the epithelium of *Sel1L*$^{\Delta IEC}$;*Ire1a*+/− mice was 6–8 fold less than that of *Sel1L*$^{\Delta IEC}$ mice, but remained 3-fold more than that of WT mice (Fig. 8d). BiP levels, both mRNA and protein, were not affected by IRE1α heterozygosity in *Sel1L*$^{\Delta IEC}$ mice (Fig. 8d–e). Moreover, treatment with a JNK-specific inhibitor SP600125 attenuated inflammation and ameliorated DSS sensitivity of *Sel1L*$^{\Delta IEC}$ mice (Supplementary Fig. 6c–f).

Both protein and mRNA levels of PERK were elevated in the gut epithelium of *Sel1L*$^{\Delta IEC}$ mice (Supplementary Fig. 7a–b), independently of IRE1α protein levels (Supplementary Fig. 7c), and so was its downstream target CHOP (Fig. 8f and Supplementary Fig. 7d). To determine the role of the PERK-CHOP axis in disease pathogenesis, we generated *Sel1L*$^{\Delta IEC}$ mice on the *Chop*−/− background (*Sel1L*$^{\Delta IEC}$;*Chop*−/−) (Supplementary Fig. 7e). Loss of *Chop* in *Sel1L*$^{\Delta IEC}$ mice had no effect on IRE1α protein level and its phosphorylation (Supplementary Fig. 7f–h). To our surprise, we found no evidence for a possible role of *Chop* in hypersensitivity to experimental colitis of *Sel1L*$^{\Delta IEC}$ mice, in terms of body weight, colon length and lesions (Fig. 8g–i). Hence, IRE1α accumulation, but not

CHOP, contributes directly to inflammation and the pathogenesis of experimental colitis in *Sel1L*$^{\Delta IEC}$ mice.

Lack of haploinsufficiency of Sel1L in vivo

Lastly, we generated *Sel1L*$^{\Delta IEC/+}$ (HET) mice as littermates to WT and *Sel1L*$^{\Delta IEC}$ mice (Supplementary Fig. 8a–b). *Sel1L*$^{\Delta IEC/+}$ mice were indistinguishable from their WT littermates, in terms of IRE1α protein level, ER stress, and sensitivity to experimental colitis (Supplementary Fig. 8c–h). As *Sel1L*$^{\Delta IEC/+}$ mice express the Cre recombinase, these data excluded a possible effect of the Cre recombinase in the disease pathogenesis of *Sel1L*$^{\Delta IEC}$ mice. Thus, one copy of Sel1L in enterocytes is sufficient for ERAD function, IRE1α degradation and colon homeostasis.

DISCUSSION

Both UPR and ERAD are evolutionarily conserved QC systems in the cell, whose coordinated activities are essential for the maintenance of ER homeostasis. However, how they are coordinated remains poorly understood. Here our data establish ERAD-mediated IRE1α protein turnover as a general self-regulatory mechanism within the ER QC systems that occurs in many cell types, both in vitro and in vivo, and is conserved from mice to humans. This study fills an important gap in the QC mechanisms by demonstrating an ingenious built-in system of “checks and balances” to dynamically fine-tune IRE1α protein level, thereby its activity and ER folding and degradation capacity, in response to dynamic fluctuation of ER homeostasis. Using an acute injury model, we further establish that ERAD-mediated IRE1α degradation is an important regulatory mechanism in restraining IRE1α signaling in enterocytes in the pathogenesis of experimental colitis in vivo (Fig. 8j).

Similar to the case of HMG-CoA reductase (HMGCR) where its degradation is high responsive to host physiology[3,34], our data demonstrate that IRE1α degradation by ERAD is highly responsive to ER homeostasis (Fig. 4g). IRE1α interacts with and is ubiquitinated by the Sel1L-Hrd1 ERAD core complex under basal conditions. The selection of IRE1α for degradation may involve BiP and OS9 as well as the intramembrane hydrophilic residues of IRE1α. ER stress triggers IRE1α-ERAD complex dissociation and hence attenuates IRE1α ubiquitination, which coincides with IRE1α dimer-/oligo-merization and activation. Our data show that the key player involved in the ER stress-mediated regulation of IRE1α protein turnover is likely to be BiP. BiP is indispensable for IRE1α degradation as depletion of BiP leads to the dissociation between IRE1α and ERAD and hence IRE1α protein stabilization while overexpression of BiP had the opposite effect. Providing further support to the key role of BiP in IRE1α degradation, dimerization-defective D123P IRE1α mutant associates constitutively with BiP and has a shorter half-life than that of WT IRE1α under stress conditions. Collectively, our data show that BiP plays a key role in targeting IRE1α for ERAD degradation under basal conditions and that ER stress triggers BiP dissociation from IRE1α and dimer-/oligomerization of IRE1α, leading to the IRE1α-ERAD complex dissociation and IRE1α protein stabilization. Hence, BiP restrains IRE1α signaling under basal conditions not only by sequestering IRE1α in an inactive state, but also by targeting it

for ERAD. This finding is consistent with the known role of BiP in substrate recruitment in ERAD[35–39].

As Sel1L-Hrd1 ERAD deficiency is intrinsically associated with the accumulation of misfolded proteins in general and hence ER stress, it may follow that the phenotypes of *Sel1L*$^{\Delta IEC}$ mice are a result of ER stress. Recent studies have also supported the role of ER stress in the pathogenesis of spontaneous and experimental colitis[17,18,40,41]. In the absence of Sel1L, ER stress is moderately induced but well tolerated by the colonic epithelium as the *Sel1L*$^{\Delta IEC}$ mice are surprisingly asymptomatic under basal conditions. Morphology of colonic epithelium and goblet cells - the major secretory cell type in the colon – appear largely normal. Thus, moderate ER stress associated with Sel1L-Hrd1 ERAD deficiency is not sufficient to alter normal physiology in the colon and induce spontaneous colitis under basal conditions. Nonetheless, *Sel1L*$^{\Delta IEC}$ mice are more susceptible to DSS-induced experimental colitis in an IRE1α-dependent and Chop-independent manner. Thus, our study reveals the pathological importance of gut epithelial Sel1L-Hrd1 ERAD and the regulation of IRE1α protein turnover in vivo. While Sel1L-Hrd1 ERAD likely has other substrates in colonic epithelium, these findings provide strong support for the notion that IRE1α degradation by ERAD is pathologically significant. This regulatory mechanism may be of great therapeutic importance as IRE1α signaling may play a critical role in intestinal inflammation[17,18].

METHODS

Mice

Sel1L$^{\Delta IEC}$, *Sel1L*$^{\Delta IEC/+}$, *Sel1L*$^{\Delta IEC}$*;Ire1a*$^{+/-}$, *Sel1L*$^{\Delta IEC}$;*Chop*$^{-/-}$, inducible Sel1L KO (*Sel1L*^{IKO}) and inducible Hrd1 KO (*Hrd1*$^{-/-}$) mice were used in this study. *Sel1L*$^{flox/flox}$, *Sel1L*$^{\Delta adipo}$, *Hrd1*$^{flox/flox}$ and *Ire1a*$^{flox/flox}$ mice were described previously[10,11,42,43]. *Sel1L*^{IKO} and inducible Hrd1 KO mice were generated using intraperitoneal injection of tamoxifen as previously described[10]. *Sel1L*$^{flox/flox}$ mice were crossed with villin-1 promoter-driven Cre mice (B6.SJL-Tg(Vil-cre)997Gum/J, JAX 004586). Different breeding schemes are shown in Supplementary Figures 3a, 6a and 8a. In addition, *Sel1L*$^{\Delta IEC}$ mice were crossed with *Chop*$^{-/-}$ mice (B6.129S(Cg)-*Ddit3*$^{tm2.1Dron}$/J, JAX 005530) to generate *Sel1L*$^{flox/flox}$*;VillinCre*$^{+}$*;Chop*$^{-/-}$ double knockout (*EKO;Chop*−/−) mice. Mice were housed under specific pathogen-free conditions and fed on a low-fat diet consisting of 13% fat, 67% carbohydrate and 20% protein (Harlan Teklad 2914). Cohoused age-matched adult littermates were used at the age of 6–12 weeks in all in vivo experiments. Animal euthanasia was performed by cervical dislocation. Tissues were immediately harvested and either fixed in 10% neutralized formalin for histology or snap-frozen in liquid nitrogen for protein and RNA analyses. Frozen tissues were stored at -80°C.

Power analysis of the animal size: Based on sample size formula of the power analysis, $N=8(CV)^2[1+(1-PC)^2]/(PC)^2$, to reach the error = 0.05, Power = 0.80, percentage change in means (PC) = 20%, co-efficient of variation (CV) = 10 ~ 15% (varies between the experiments), 5 mice per group are the minimal number of mice to obtain statistical significance. Hence, in general, we used a total of 5 mice in each study to ensure adequate power. Mice in each group were randomly chosen based on the age, genotype and gender.

All animal procedures have been approved by the Institutional Animal Care and Use Committee (IACUC) at Cornell University and Northwestern University.

Cell lines

Sel1L$^{flox/flox}$*;ERCre*$^{+}$ MEFs were generated and Se11L deletion was induced by treating with 400 nM 4-Hydroxytamoxifen (4-OHT, Sigma H7904) as previously described[10]. In some studies, parental *Sel1L*$^{flox/flox}$*;ERCre*$^{+}$ MEFs were transfected to stably express pcDNA3-His-Myc-HRD1 using Lipofectamine 2000 (Invitrogen) per supplier's protocol. 24 h later, cells were selected with 400 μg/ml G418 (EMD Millipore) and G418-resistant cells were expanded for further analysis. These cells were treated with 4-OHT or vehicle as described above to delete Sel1L. Hrd1−/− and WT MEFs were kindly provided by Dr. Toshihiro Nakajima (Tokyo Medical University)[44]. IRE1α−/− MEFs stably expressing pMSCV-hIRE1α-HA (WT or D123P mutant) were previously described[26]. All cells including HEK293T and MEFs were maintained in DMEM (Cellgro, Herndon, VA) supplemented with 10% FBS (Sigma) and 1% penicillin-streptomycin (Cellgro). Mouse intestinal m-IC$_{cl2}$ cells were a kind gift from Dr. Judith Appleton (Cornell) and were cultured as previously described[45]. For stable shRNA knockdown, Sel1L and Hrd1 shRNA targeting sequences (GGTTACACTGTGGCTAGAA and GGAGAGTTTCAGATGATTA) were cloned into pSuper/retro vector (H1 promoter). Control RNAi were against the firefly luciferase. m-IC$_{cl2}$ cells stably expressing XBP1s were generated using retroviral transduction as previously described[27]. MEFs expressing BiP- or control LacZ were generated using adenoviral infection at 1,000 multiplicity of infection (MOI) per well of a 6 well plate (adenoviruses were kindly provided by Drs. Heinrich Lob and Robin Davisson at Cornell University). 4 days after infection, cells were treated with 300 nM Tg for 12 h and snap-frozen for Western blot.

CRISPR-based knockout cell lines

CRISPR targeting oligos designed for human SEL1L (#1 ACTGCAGGCAGAGTAGTTGC, #2 GACATCAGATGAGTCAGTAA) and human OS9 (5'GCAAGTCTGACCGGCGGTGTC) were inserted into the pX330-U6-Chimeric_BB-CBh-hSpCas9 vector (Addgene 42230). Oligos targeting mouse Xbp1 (GCTCATGGTACCCGGTCCGC) and mouse Ire1α (CTTGTTGTTTGTCTCGACCC) were used in m-ICc12 cells. Cells were co-transfected with CRISPR constructs, together with the pBabe-puro vector, and selected with 2 or 3 μg/ml puromycin (Invitrogen) for 48 h. Surviving cells were plated to 96-wells with one cell per well for single colony selection. Knockout efficiency in HEK293T cells was assessed by Western blot analysis. In m-ICc12 cells, knockout lines were sequenced using primer sets GCCCCCAAAGTGCTACTCTTA and CCGTGAGTTTTCTCCCGTAA for Xbp1 and TTTTGGAAGAACCAGCACAG and GCCAGTCAGGAGGTCGATAA for Ire1α.

Transmission electron microscopy (TEM)

Sel1L$^{flox/flox}$*;ERCre*$^{+}$ MEFs were treated with vehicle (WT) or 4-OHT (*Sel1L*^{IKO}) for 3 days, harvested and fixed as cell pellets. Samples were stained, dehydrated, and processed as described before[10].

ER purification and precipitation

ER purification was performed as previously described[46]. Briefly, *Sel1L*$^{flox/flox}$*;ERCre*$^{+}$ MEFs were treated with 4-OHT or vehicle for 4 days. Subsequent steps were performed at 4°C in the presence of the protease inhibitor cocktail (Sigma). A total of 1×10^7 cells were homogenized in Dounce grinder with buffer A (50 mM Tris-HCl pH 8.0, 1 mM β-mercaptoethanol, 1 mM EDTA, and 0.32 M sucrose), and then centrifuged at 5,000 g for 10 min. The supernatant was centrifuged at 105,000 g for 1 h (XL-80K, Beckman). The pellet was disrupted in lysis buffer (50 mM Tris-HCl pH 7.5, 150 mM NaCl, 1% NP-40, 1 mM dithiothreitol, 1 mM sodium orthovanadate and 10 mM sodium fluoride) followed by centrifugation at 15,000 g for 20 min. The resulting supernatant, the ER fraction, was quantitated using the Bradford assay and adjusted to the same protein concentration. 200 μL ER fraction was precipitated by methanol and chloroform and subjected to mass spectrometric analysis.

Mass spectrometry

Mass spectrometry to identify ERAD substrates was performed previously described[47].

Protein lysate preparation, Western blot and quantitation

Preparation of cell and tissue lysates and Western blot were performed as previously described[27]. IRE1α phosphorylation was measured by a Phos-tag-based Western blot method[27–29]. For non-reducing SDS-PAGE, lysates were prepared in 5 X non-denaturing sample buffer (250 mM Tris HCl pH 6.8, 1% SDS, 50% glycerol and 0.05% bromophenyl blue) without boiling prior to be separated on a SDS-PAGE gel. Antibodies used in this study were: HSP90 (sc-7947, 1:6,000), GFP (sc-8334, 1:2000), BiP (sc-1051, 1:1,000), IRE1β (sc-20575, 1:1000), JNK1 (sc-571, 1:1000), α-Tubulin (sc-5286, 1:2000) from Santa Cruz; IRE1α (#3294, 1:2000), PERK (#3192, 1:2,000), Caspase-3 (#9665, 1:1000), p-T183/Y185-JNK (#9255, 1:2000), from Cell Signaling; Sel1L (ab78298, 1:2,000), OS9 (ab109510, 1:10,000) from Abcam; Hrd1 (NB100-2526, 1:8,000) from Novus Biologicals; Calnexin (SPA-860, 1:8,000) and PDIA1 (SPA-890, 1:8,000) from Enzo Life Sciences; Flag-HRP (A-8592, 1:8,000), HA (H9658, 1:5,000) from Sigma. Antibodies for Bag6 (rabbit, 1:10,000) and H2A (rabbit, 1:10,000) were kind gifts from Dr. Yihong Ye (NIDDK). Band density was quantitated using the Image Lab software on the ChemiDOC XRS^{+} system (Bio-Rad). Protein levels were normalized to HSP90 or α-Tubulin and are presented as mean ± s.e.m. unless otherwise specified.

Immunoprecipitation (IP)

Cells were lysed in lysis buffer (150 mM NaCl, 1mM EDTA, 50 mM Tris HCl pH 7.5 or 8.0, protease inhibitor and protein phosphatase inhibitor and 10 mM N-ethymaleimide) supplemented with 1% Triton X-100 or 1% Nonidet P-40 (NP-40). A total of ~ 2 mg protein lysates was incubated with 2 μl primary or irrelevant antibody overnight at 4°C with gentle rocking. Antibodies used for IP: IRE1α (Cell Signaling, #3294), GFP (Santa Cruz, sc-8334), and normal rabbit IgG (Santa Cruz, sc-2027). Immunocomplexes were precipitated with protein A-agarose beads (Invitrogen, 15918014) for 8 h at 4°C, washed and eluted by boiling for 5 min in 2 X SDS sample buffer. For immunoprecipitation of tagged proteins, lysates

were immunoprecipitated overnight at 4°C with HA- (Sigma, A2095) or FLAG-agarose beads (Sigma, A2220). For denaturing IP, HEK293T cells transfected with indicated plasmids in each 10 cm dish were lysed in 200 μl NP-40 lysis buffer with 1% SDS and 5 mM DTT, and denatured at 95°C for 10 min. Subsequently, samples were diluted 1:10 with NP-40 lysis buffer followed by IP as described above.

Substrate competition

HEK293FT cells were transfected with empty vector or pEGFP-N1 plasmid (Clontech) containing NHK-GFP using Lipofectamine 2000 (Invitrogen) per manufacturer's instruction. Two days after transfection, cells were snap frozen in liquid nitrogen. IP was carried out as described above.

In vitro drug treatment

Thapsigargin (Tg), tunicamycin (Tm) and MG132 were purchased from Millipore, dissolved in DMSO and used at 150–300 nM, 2.5 μg/ml, and 10 μM, respectively. Cycloheximide (CHX, Millipore) was dissolved in ethanol and used at 50 μg/ml. To evaluate inflammatory responses, cells were treated with 50 ng/ml murine TNFα for 10 min with or without 1 h pretreatment with 50 μM SP600125[48]. SubAB and its catalytic inactive mutant form $SubA_{A272}B$ were used at 1 μg/ml as previously described[24].

Plasmids

(h denotes human genes; m denotes mouse genes): pCMV-Tag4A-hIRE1α-Flag (gift from Dr. Yong Liu, Institute of Nutritional Sciences, China)[49]; pcDNA3-His-Myc-hHrd1 WT and ring-finger mutant C2A (C291A/C294A) (gifts from Dr. Yihong Ye, NIDDK)[19]; pcDNA3-HA-Ub and pcDNA3-HA-hSel1L plasmids (gifts from Dr. Hideki Nishitoh, University of Miyazaki). IRE1α T3A mutants (T446A, S450A and T451A) were generated using site-directed mutagenesis of pCMV-Tag4A-hIRE1α-Flag and mutagenesis primers are Forward: 5' CTTAAGGACATGGCTGCCATCATCCTGGCCGCCTTCCTGCTGATTG, Reverse 5'CAATCAGCAGGAAGGCGGCCAGGATGATGGCAGCCATGTCCTTAAG.

Sucrose gradient sedimentation analysis

Confluent WT MEFs in two 10 cm plates either mock-treated or treated with 300 nM Tg for 4 h were lysed in 0.5ml 1% NP40 lysis buffer. Extracts were centrifuged through 20%– 40% sucrose gradients (in 150 mM NaCl, 1mM EDTA, 50 mM Tris HCl pH 7.5 and protease inhibitor) prepared freshly by progressively layering higher to lower density sucrose fractions in 5% increments. Extracts were centrifuged at 58,000 rpm for 14.5 hours at 4°C using an SW 60 Ti rotor (Beckman Coulter). Each 4 ml gradient was divided evenly into 10 fractions (400 μl each), and aliquots of fractions 5–10 were subjected to Western blot analyses under denaturing or non-denaturing conditions.

Limited proteolysis

HEK293T cells were incubated in the absence or presence of 100 nM Tg for 3 h, harvested, and lysed in lysis buffer containing 50 mM HEPES (pH=7.5), 150 mM NaCl and 1% Triton-X 100 on ice for 15 min. Aliquots of the lysates were mixed with various concentrations of

trypsin and incubated on ice for 30 min. Reaction was quenched by adding SDS sample buffer and immediately heated at 95°C for 10 min followed by Western blot analysis.

Pulse labeling and pulse-chase analysis

Cells transfected with Flag-IRE1α or HA-IRE1α were cultured with cysteine and methionine-free medium (Invitrogen, 21013024) containing 10 mM HEPES, pH 7.4 at 37°C for 30 min and pulse labeled with 100 μCi/ml [^{35}S]-cysteine and methionine (EasyTag, PerkinElmer) at 37°C for 30 min. In the pulse-chase assay, following 30 min pulse, cells were cultured in chase medium (10 mM HEPES, 5 mM cysteine, 5 mM methionine) for the indicated time in the presence or absence of 300 nM Tg. Cells were then extensively washed with ice-cold HBSS buffer (Gibco, Life Technologies) and snap-frozen in liquid nitrogen. Cells were lysed and immunoprecipitated as described above using NP-40 as detergent. Lysates were separated on a 7% SDS-PAGE gel, which was subsequently incubated with the neutralizing buffer (30% (v/v) methanol in PBS) for 10 min followed by the enhancer buffer (1.5 M sodium salicylate (Sigma) in 30% (v/v) methanol) for 10 min. The gel was then dried at 80°C for 2 h using a gel drier (Model 583, Bio-Rad) and subjected to autoradiography with X-film (Kodak).

Histological analysis

Tissues were fixed in 10% neutralized formalin and processed by the Cornell Histology Core Facility on a fee-for-service basis. Hematoxylin and eosin (H&E) slides were photographed as previously described[10]. Tissue sections were examined blindly by a board-certified anatomic pathologist (G.E.D.). For the assessment of the severity of experimental colitis, histological scores of the distal colon were blindly determined based on globet cell loss, crypt abscesses, immune cell infiltration and epithelial erosion (0, none; 1, low; 2, moderate; 3, high; 4, maximal) as previously described[50]. Of note, other animal experiments were not performed blindly.

Animal experiments

High through-put sequencing of 16S rRNA V4 region of fecal pellets from cohoused 8-week-old mice were performed as previously described[51]. Mice were fed ad libitum with 3% (wt/vol) DSS (molecular weight 40–50 kDa; Affymetrix, Santa Clara, CA) dissolved in drinking water for 5 days and then fresh water thereafter. Body weights were monitored every other day until the end of experiments. Stool consistency (0, normal; 1, soft but still formed; 2, very soft; 3, diarrhea) and stool blood (0, negative; 1, positive hemoccult; 2, blood traces in stool visible; 3, rectal bleeding) were assessed on day 6 after DSS treatment started[50]. At day 7, flow cytometric analysis of activated CD8+ T cells was performed as previously described[52] and serum cytokine levels were measured using the Bio-Plex Pro™ Mouse Cytokine 9- and 23-plex Assay and the Bio-Plex MAGPIX™ system (Bio-Rad #M6009RDPD) per manufacture's instruction. For antibiotic treatment, mice were given ampicillin (1 g/l; Fisher) and neomycin sulfate (1 g/l; Cellgro) dissolved in drinking water during and after DSS treatment. For humane reasons and IACUC guidelines, mice were declared "dead" and were euthanized when body weight dropped by 20%. SP600125 (LC Laboratories), a JNK-specific inhibitor[48], was dissolved in 7% Kolliphor™ Solutol HS-15 (Sigma, in PBS) at 3 mg/ml. Age-matched littermates were injected intraperitoneally with

SP600125 or vehicle at a volume of 10 μl/g body weight every other day with concurrent 5-day 3% DSS feeding regimen until the end of the experiment. Mice were monitored daily and body weights were measured every other day.

Colonic epithelium isolation

After removing surrounding fat and connective tissues, the colon was cut longitudinally into small pieces shaken in 5 mL PBS containing 30mM EDTA at 37°C for 20 min. Colonic epithelial cells were released by vortexing at max setting for 15 sec twice and collected from supernatant. Purified cells were used for protein, mRNA and microarray analyses. The purity of colonic epithelial cells was examined using RT-PCR analysis of the enterocyte-specific gene villin and leukocyte-specific gene CD45.

Organoid culture

Small intestine crypts were isolated and cultured as described previously[53]. Briefly, small intestines from adult mice were rinsed with ice-cold PBS, cut longitudinally and shaken vigorously in ice-cold PBS to remove villi. Tissues were cut into small pieces and shaken gently in 30 ml PBS containing 2 mM EDTA at 4°C for 1 h. Crypts were released by vigorous shaking and were pelleted at 230 rcf for 2 min at 4°C. Isolated crypts were mixed with Matrigel (Corning), plated in 24-well plates, and cultured in crypt culture medium (Advanced DMEM/F12, Invitrogen) containing growth factors (50 ng/ml EGF (Invitrogen), 500 ng/ml R-spondin-1 (R&D) and 100 ng/ml Noggin (Peprotech)). For drug treatment, organoids were either treated with 25 μg/ml CHX for 2 h or 50 ng/ml murine TNFα for 20 min, then removed from Matrigel mechanically in ice-cold PBS and pelleted immediately for protein or RNA extraction.

Immunohistochemistry (IHC)

Formalin-fixed, paraffin-embedded intestinal sections were processed for IHC and TUNEL staining as previously described[10]. IHC was performed with the Histostain kit and DAB substrate from Invitrogen. Primary antibodies used for IHC were IRE1α (#3294, 1:100) from Cell Signaling and OS9 (ab109510, 1:200) from Abcam. Sections were scanned and images were taken using the Aperio Scanscope. TUNEL staining was performed with the in Situ Death Detection TUNEL Kit (Roche 11684795910). The fluorescence was visualized and images were captured under a Zeiss LSM710 confocal microscope with 10× magnification at Cornell Biotechnology Resource Center Imaging Facility.

FISH

Formalin-fixed paraffin-embedded intestine sections were mounted on Probe-On Plus slides (Fisher) and evaluated by FISH with probes to all bacteria (EUB338-5'Cy3) or *E.coli/Shigella* (*E.coli*-5'Cy3, 16S rRNA), in combination with a non-specific binding control probe (non-EUB338-5'FAM) (IDT, Coralville, IA), as previously described[32]. Sections were examined with an Olympus BX51 fluorescence microscope and images were captured with an Olympus DP-7 camera.

Immunocytochemistry

HEK293T cells were plated on poly-L-lysine-coated coverslips and transfected with Flag-IRE1α WT or T3A mutant plasmids for 24 h. Cells were processed and labeled with anti-IRE1α (#3294, Cell Signaling) and anti-BiP (sc-1051, Santa Cruz) as previously described[47]. Cells were then labeled with donkey anti-rabbit AF594 (711-585-152) and donkey anti-goat AF680 (705-625-147) from Jackson ImmunoResearch, and mounted with Prolong Gold Antifade Reagent with DAPI (Invitrogen). Fluorescent microscopic images were taken under a Zeiss LSM710 confocal microscope at Cornell Biotechnology Resource Center Imaging Facility.

NP-40 solubility assay

Frozen terminal ileum tissue was weighed and homogenized in NP-40 lysis buffer as previously described[10]. The lysate volume was normalized by tissue weight, centrifuged at 12,000 × g for 10 min and the supernatant was collected as NP-40S fraction. The pellet was then resuspended in 1× SDS sample buffer with the volume normalized to initial tissue weight, heated at 95°C for 30 min and collected as the NP-40P fraction.

RNA extraction, RT-PCR for *Xbp1* mRNA splicing and qPCR

Total RNA were extracted from mouse tissues and cells using Trizol and RNA miniprep kit (Sigma RTN350) with DNaseI digestion (New England Biolabs). RNA quality was determined by measuring the OD260/280 and visualized on an agarose gel. RT-PCR were performed as previously described[27]. Percent of *Xbp1* mRNA splicing defined as the ratio of *Xbp1s* level to total *Xbp1* (*Xbp1u +Xbp1s*) levels was quantitated using the ImageLab software. All qPCR data for mouse tissues and cells were normalized to ribosomal *l32* gene in the corresponding sample. Q-PCR primer sequences (forward, reverse) are: (mouse genes if not specified)

Ire1a (CTGTGGTCAAGATGGACTGG, GAAGCGGGAAGTGAAGTAGC),

Ire1b (CCGCTCATACAAAGGGACAT, ATGAAGCCAGCAGGAAGTTG),

Xbp1s (GAGTCCGCAGCAGGTG, GTGTCAGAGTCCATGGGA),

Perk (TCAAGTTTCCTCTACTGTTCACTCA, CGGGAAACTCCAAGTTCTCA),

Chop (TATCTCATCCCCAGGAAACG, GGGCACTGACCACTCTGTTT),

BiP (TGTGGTACCCACCAAGAAGTC, TTCAGCTGTCACTCGGAGAAT),

Erdj4 (CTTAGGTGTGCCAAAGTCTGC, GGCATCCGAGAGTGTTTCATA),

Sel1l (TGGGTTTTCTCTCTCTCCTCTG, CCTTTGTTCCGGTTACTTCTTG),

Hrd1 (AGCTACTTCAGTGAACCCCACT, CTCCTCTACAATGCCCACTGAC),

Os9 (GCTCACGCCTACTACCTCAAA, GCCAGACAAGTCTCTGTGACG),

Edem1 (GGGACCAAGAGGAAAAGTTTG, GAGGTGAGCAGGTCAAATCAA),

Pdia6 (TGGTTCCTTTCCTACCATCACT, ACTTTCACTGCTGGAAAACTGC),

Tnfa (TCAGCCGATTTGCTATCTCATA, AGTACTTGGGCAGATTGACCTC),

L32 (GAGCAACAAGAAAACCAAGCA, TGCACACAAGCCATCTACTCA),

Human IRE1a (AGAGAAGCAGCAGACTTTGTC, GTTTTGGTGTCGTACATGGTGA),

Human OS9 (GCTCACGCCTACTACCTCAAA, GCCAGACAAGTCTCTGTGACG),

Human L32 (AGTTCCTGGTCCACAACGTC, TTGGGGTTGGTGACTCTGAT).

Human Xbp1 splicing (CTGGAACAGCAAGTGGTAGA, CTGGGTCCTTCTGGGTAGAC).

Microarray analysis

Colon epithelium was isolated from 8-week-old WT and $Sel1L^{\Delta IEC}$ male mice and snap frozen in liquid nitrogen (n=4 each). RNA was extracted as described above. RNA quality and concentration were determined using the RNA 6000 Nano kit on an Agilent 2100 bioanalyzer. The cDNA array of colonic RNA was prepared as previously described[54].

Statistical analysis

Results are expressed as mean ± SEM. Comparisons between groups were made by unpaired two-tailed Student's *t* test unless otherwise indicated. Survival curves were compared by the Log-rank (Mantel-Cox) test. $P < 0.05$ was considered statistically significant. All experiments were repeated at least twice or performed with independent samples. Representative data are shown.

Supplementary Material

Refer to Web version on PubMed Central for supplementary material.

ACKNOWLEDGEMENTS

We thank for Kuei-Ling Tung for help with the organoid culture; and other members of the Qi lab for comments and technical assistance. S.S. is an International Student Research Fellow of the Howard Hughes Medical Institute (59107338). L.Q. is the recipient of the Junior Faculty and Career Development Awards from American Diabetes Association (ADA). This work was supported by R21AI085332 (G.D.), 1R03AI114344 (H.W.), Chinese National Natural Science Foundation Grant 31371391 (Q. L.), National Heart, Lung, and Blood Institute Proteomics Center Award HHSN268201000035C, R01 MH067880 and 8P41GM103533-17 (J.R.Y), NIH R01DK105393, R01GM113188, UL1TR000457 of the Clinical and Translation Science Center at Weill Cornell Medical College, ADA 1-12-CD-04 and Cornell VERG seed grant (L.Q.).

REFERENCES

1. Guerriero CJ, Brodsky JL. The delicate balance between secreted protein folding and endoplasmic reticulum-associated degradation in human physiology. Physiol Rev. 2012; 92:537–576. [PubMed: 22535891]
2. Olzmann JA, Kopito RR, Christianson JC. The Mammalian Endoplasmic Reticulum-Associated Degradation System. Cold Spring Harbor perspectives in biology. 2013; 5
3. Hampton RY, Gardner RG, Rine J. Role of 26S proteasome and HRD genes in the degradation of 3-hydroxy-3-methylglutaryl-CoA reductase, an integral endoplasmic reticulum membrane protein. Mol Biol Cell. 1996; 7:2029–2044. [PubMed: 8970163]
4. Christianson JC, et al. Defining human ERAD networks through an integrative mapping strategy. Nat Cell Biol. 2012; 14:93–105. [PubMed: 22119785]

5. Mueller B, Lilley BN, Ploegh HL. SEL1L, the homologue of yeast Hrd3p, is involved in protein dislocation from the mammalian ER. J Cell Biol. 2006; 175:261–270. [PubMed: 17043138]
6. Gardner RG, et al. Endoplasmic reticulum degradation requires lumen to cytosol signaling. Transmembrane control of Hrd1p by Hrd3p. J Cell Biol. 2000; 151:69–82. [PubMed: 11018054]
7. Plemper RK, et al. Genetic interactions of Hrd3p and Der3p/Hrd1p with Sec61p suggest a retro-translocation complex mediating protein transport for ER degradation. J Cell Sci. 1999; 112(Pt 22): 4123–4134. [PubMed: 10547371]
8. Carvalho P, Goder V, Rapoport TA. Distinct ubiquitin-ligase complexes define convergent pathways for the degradation of ER proteins. Cell. 2006; 126:361–373. [PubMed: 16873066]
9. Mueller B, Klemm EJ, Spooner E, Claessen JH, Ploegh HL. SEL1L nucleates a protein complex required for dislocation of misfolded glycoproteins. Proc Natl Acad Sci USA. 2008; 105:12325–12330. [PubMed: 18711132]
10. Sun S, et al. Sel1L is indispensable for mammalian endoplasmic reticulum-associated degradation, endoplasmic reticulum homeostasis, and survival. Proc Natl Acad Sci U S A. 2014; 111:E582–E591. [PubMed: 24453213]
11. Sha H, et al. The ER-associated degradation adaptor protein Sel1L regulates LPL secretion and lipid metabolism. Cell Metab. 2014; 20:458–470. [PubMed: 25066055]
12. Bertolotti A, Zhang Y, Hendershot LM, Harding HP, Ron D. Dynamic interaction of BiP and ER stress transducers in the unfolded-protein response. Nat Cell Biol. 2000; 2:326–332. [PubMed: 10854322]
13. Mori K, Ma W, Gething MJ, Sambrook J. A transmembrane protein with a cdc2+/CDC28-related kinase activity is required for signaling from the ER to the nucleus. Cell. 1993; 74:743–756. [PubMed: 8358794]
14. Cox JS, Shamu CE, Walter P. Transcriptional induction of genes encoding endoplasmic reticulum resident proteins requires a transmembrane protein kinase. Cell. 1993; 73:1197–1206. [PubMed: 8513503]
15. Walter P, Ron D. The unfolded protein response: from stress pathway to homeostatic regulation. Science. 2011; 334:1081–1086. [PubMed: 22116877]
16. He Y, et al. Emerging roles for XBP1, a sUPeR transcription factor. Gene Expr. 2010; 15:13–25. [PubMed: 21061914]
17. Kaser A, et al. XBP1 links ER stress to intestinal inflammation and confers genetic risk for human inflammatory bowel disease. Cell. 2008; 134:743–756. [PubMed: 18775308]
18. Adolph TE, et al. Paneth cells as a site of origin for intestinal inflammation. Nature. 2013; 503:272–276. [PubMed: 24089213]
19. Kikkert M, et al. Human HRD1 is an E3 ubiquitin ligase involved in degradation of proteins from the endoplasmic reticulum. J Biol Chem. 2004; 279:3525–3534. [PubMed: 14593114]
20. Kim W, Spear ED, Ng DT. Yos9p detects and targets misfolded glycoproteins for ER-associated degradation. Mol Cell. 2005; 19:753–764. [PubMed: 16168371]
21. Bhamidipati A, Denic V, Quan EM, Weissman JS. Exploration of the topological requirements of ERAD identifies Yos9p as a lectin sensor of misfolded glycoproteins in the ER lumen. Mol Cell. 2005; 19:741–751. [PubMed: 16168370]
22. Sato BK, Schulz D, Do PH, Hampton RY. Misfolded membrane proteins are specifically recognized by the transmembrane domain of the Hrd1p ubiquitin ligase. Mol Cell. 2009; 34:212–222. [PubMed: 19394298]
23. Gething MJ. Role and regulation of the ER chaperone BiP. Semin Cell Dev Biol. 1999; 10:465–472. [PubMed: 10597629]
24. Paton AW, et al. AB5 subtilase cytotoxin inactivates the endoplasmic reticulum chaperone BiP. Nature. 2006; 443:548–552. [PubMed: 17024087]
25. Zhou J, et al. The crystal structure of human IRE1 luminal domain reveals a conserved dimerization interface required for activation of the unfolded protein response. Proc Natl Acad Sci USA. 2006; 103:14343–14348. [PubMed: 16973740]
26. Xue Z, et al. A conserved structural determinant located at the interdomain region of mammalian inositol-requiring enzyme 1alpha. J Biol Chem. 2011; 286:30859–30866. [PubMed: 21757700]

27. Sha H, et al. The IRE1alpha-XBP1 pathway of the unfolded protein response is required for adipogenesis. Cell Metab. 2009; 9:556–564. [PubMed: 19490910]
28. Qi L, Yang L, Chen H. Detecting and quantitating physiological endoplasmic reticulum stress. Meth Enzymol. 2011; 490:137–146. [PubMed: 21266248]
29. Yang L, et al. A Phos-tag-based method reveals the extent of physiological endoplasmic reticulum stress. PLos ONE. 2010; 5:e11621. [PubMed: 20661282]
30. Okayasu I, et al. A novel method in the induction of reliable experimental acute and chronic ulcerative colitis in mice. Gastroenterology. 1990; 98:694–702. [PubMed: 1688816]
31. Dogan B, et al. Inflammation-associated adherent-invasive Escherichia coli are enriched in pathways for use of propanediol and iron and M-cell translocation. Inflamm Bowel Dis. 2014; 20:1919–1932. [PubMed: 25230163]
32. Craven M, et al. Inflammation drives dysbiosis and bacterial invasion in murine models of ileal Crohn's disease. PLoS ONE. 2012; 7:e41594. [PubMed: 22848538]
33. Redl H. Cytokines in Severe Sepsis and Septic Shock. Birkhäuser. 2013
34. Goldstein JL, Brown MS. Regulation of the mevalonate pathway. Nature. 1990; 343:425–430. [PubMed: 1967820]
35. Ushioda R, Hoseki J, Nagata K. Glycosylation-independent ERAD pathway serves as a backup system under ER stress. Mol Biol Cell. 2013; 24:3155–3163. [PubMed: 23966469]
36. Zhang T, Ye Y. The final moments of misfolded proteins en route to the proteasome. DNA and cell biology. 2014; 33:477–483. [PubMed: 24833120]
37. Plemper RK, Bohmler S, Bordallo J, Sommer T, Wolf DH. Mutant analysis links the translocon and BiP to retrograde protein transport for ER degradation. Nature. 1997; 388:891–895. [PubMed: 9278052]
38. Brodsky JL, et al. The requirement for molecular chaperones during endoplasmic reticulum-associated protein degradation demonstrates that protein export and import are mechanistically distinct. J Biol Chem. 1999; 274:3453–3460. [PubMed: 9920890]
39. Okuda-Shimizu Y, Hendershot LM. Characterization of an ERAD Pathway for Nonglycosylated BiP Substrates, which Require Herp. Mol Cell. 2007; 28:544–554. [PubMed: 18042451]
40. Park SW, et al. The protein disulfide isomerase AGR2 is essential for production of intestinal mucus. Proc Natl Acad Sci U S A. 2009; 106:6950–6955. [PubMed: 19359471]
41. Zhao F, et al. Disruption of Paneth and goblet cell homeostasis and increased endoplasmic reticulum stress in Agr2−/− mice. Dev Biol. 2010; 338:270–279. [PubMed: 20025862]
42. Wu T, et al. Hrd1 suppresses Nrf2-mediated cellular protection during liver cirrhosis. Genes Dev. 2014; 28:708–722. [PubMed: 24636985]
43. Iwawaki T, Akai R, Yamanaka S, Kohno K. Function of IRE1 alpha in the placenta is essential for placental development and embryonic viability. Proc Natl Acad Sci USA. 2009; 106:16657–16662. [PubMed: 19805353]
44. Yagishita N, et al. Essential role of synoviolin in embryogenesis. J Biol Chem. 2005; 280:7909–7916. [PubMed: 15611074]
45. Bens M, et al. Transimmortalized mouse intestinal cells (m-ICc12) that maintain a crypt phenotype. The American journal of physiology. 1996; 270:C1666–C1674. [PubMed: 8764149]
46. Sheng YH, et al. The MUC13 cell-surface mucin protects against intestinal inflammation by inhibiting epithelial cell apoptosis. Gut. 2011; 60:1661–1670. [PubMed: 21636645]
47. He Y, et al. Non-muscle myosin IIB links cytoskeleton to IRE1α signaling during ER stress. Dev Cell. 2012; 23:1141–1152. [PubMed: 23237951]
48. Bennett BL, et al. SP600125, an anthrapyrazolone inhibitor of Jun N-terminal kinase. Proc Natl Acad Sci U S A. 2001; 98:13681–13686. [PubMed: 11717429]
49. Qiu Y, et al. A crucial role for RACK1 in the regulation of glucose-stimulated IRE1alpha activation in pancreatic beta cells. Science Signaling. 2010; 3:ra7. [PubMed: 20103773]
50. Wirtz S, Neufert C, Weigmann B, Neurath MF. Chemically induced mouse models of intestinal inflammation. Nat Protoc. 2007; 2:541–546. [PubMed: 17406617]
51. Ji Y, et al. Diet-Induced Alterations in Gut Microflora Contribute to Lethal Pulmonary Damage in TLR2/TLR4-Deficient Mice. Cell reports. 2014; 8:137–149. [PubMed: 24953658]

52. Xia S, et al. Gr-1+ CD11b+ Myeloid-derived Suppressor Cells Suppress Inflammation and Promote Insulin Sensitivity in Obesity. J Biol Chem. 2011; 286:23591–23599. [PubMed: 21592961]

53. Sato T, et al. Single Lgr5 stem cells build crypt-villus structures in vitro without a mesenchymal niche. Nature. 2009; 459:262–265. [PubMed: 19329995]

54. Sun S, Xia S, Ji Y, Kersten S, Qi L. The ATP-P2X7 Signaling Axis Is Dispensable for Obesity-Associated Inflammasome Activation in Adipose Tissue. Diabetes. 2012; 61:1471–1478. [PubMed: 22415881]

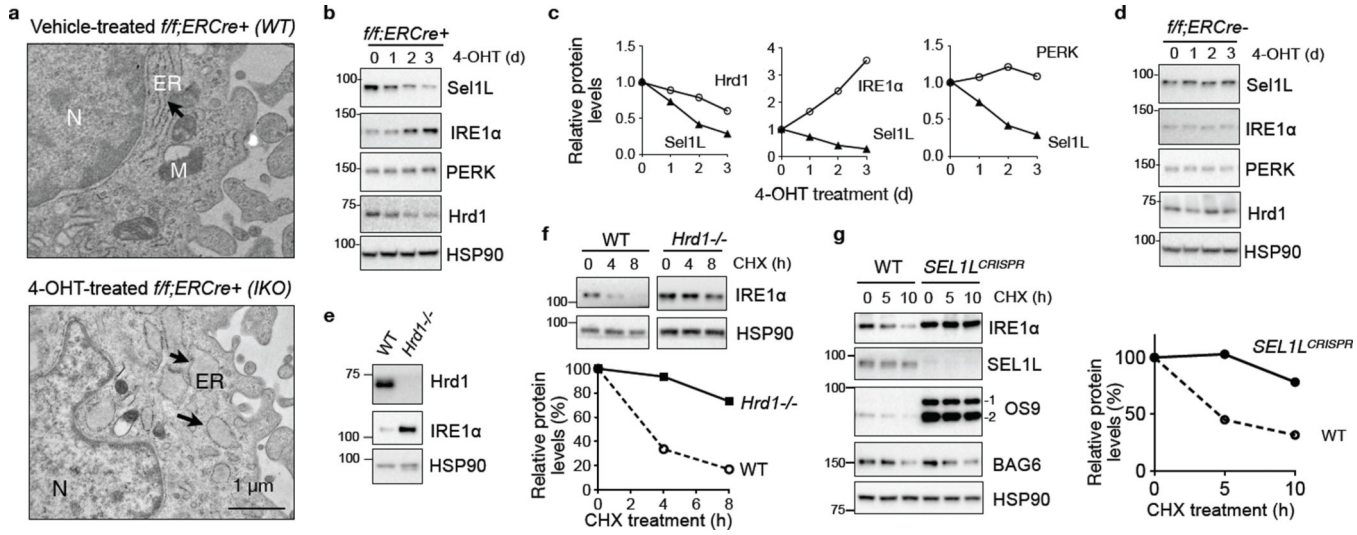

Figure 1. IRE1α is a Sel1L-Hrd1 substrate in vitro

(a) Representative TEM images of *Sel1Lf/f;ERCre+* MEFs treated with vehicle (WT) or 4-OHT (IKO) for 3 days. ER, endoplasmic reticulum (arrows); M, mitochondrion; N, nucleus. **(b–c)** Western blot analysis of *Sel1Lf/f;ERCre+* (*f/f;ERCre+*) MEFs treated with 4-OHT for the indicated time **(b)**, with quantitation shown in **(c)**. **(d)** Western blot analysis of *Sel1Lf/f;ERCre−* MEFs treated with 4-OHT. **(e)** Western blot analysis of IRE1α in WT and Hrd1−/− MEFs, with quantitation shown in Supplementary Fig. 1e. **(f)** Western blot analysis of IRE1α in MEFs treated with 50 μg/ml cycloheximide (CHX) for the indicated time, with quantitation shown below. **(g)** Western blot analysis of IRE1α in CHX-treated WT and SEL1L-deficient (*SEL1L*^{CRISPR}) HEK293T cells, with quantitation shown on the right. The ERAD substrate OS9 and the cytosolic proteins BAG6 and HSP90 are shown as controls. Representative data from three independent experiments shown. Unprocessed original scans of blots are shown in Supplementary Fig. 9.

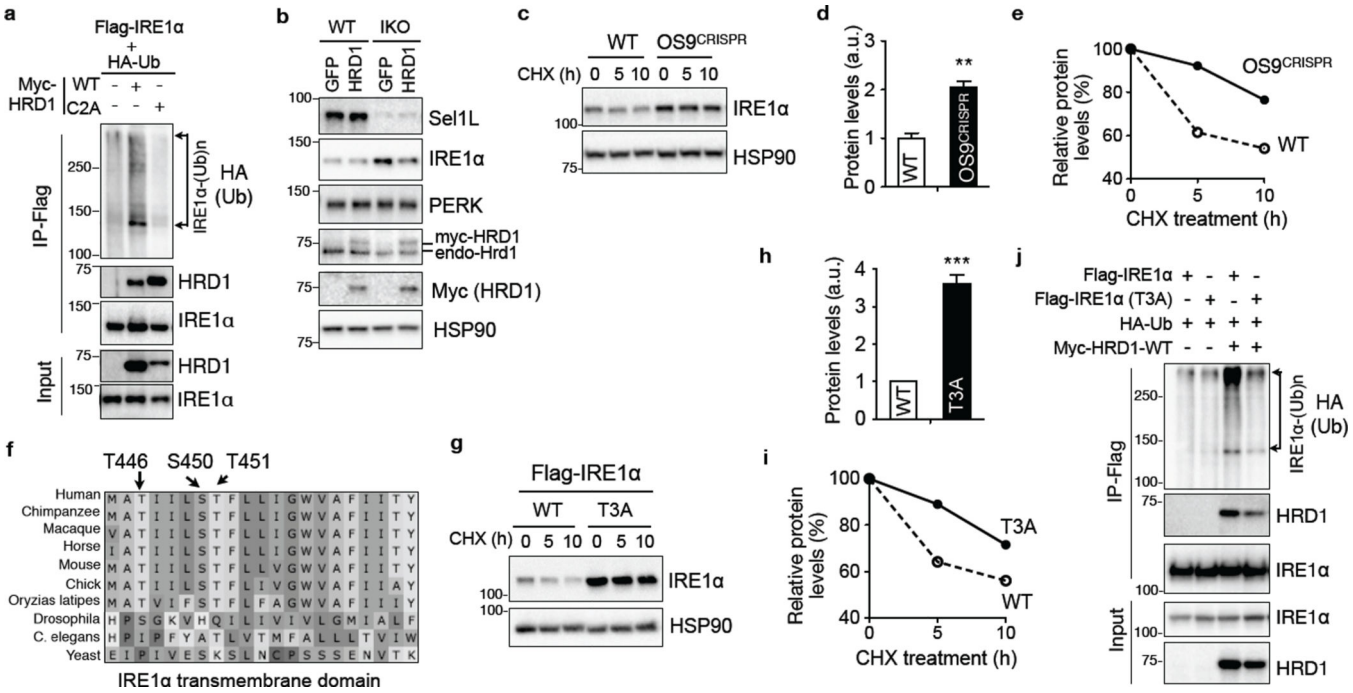

Figure 2. The role of OS9 and intramembrane hydrophilic residues of IRE1α in Sel1L-Hrd1-mediated IRE1α degradation

(**a**) Western blot analysis of immunoprecipitates of Flag-agarose in transfected HEK293T, showing the ubiquitination of IRE1α by HRD1 in vitro. (**b**) Western blot analysis of IRE1α in WT and IKO MEFs stably expressing HRD1-myc, with quantitation shown in Supplementary Fig. 2b. (**c–e**) Western blot analysis of IRE1α decay in CHX-treated WT and OS9-deficient (OS9^{CRISPR}) HEK293T cells, with quantitation of total protein at basal state and protein decay shown in (**d**) and (**e**), respectively. (**f**) Alignment of IRE1α transmembrane domain (444–464aa) across species showing three hydrophilic residues. (**g–i**) Western blot analysis of IRE1α in CHX-treated HEK293T cells transfected with WT and T3A Flag-IRE1α, with quantitation of total protein at basal state and protein decay shown in (**h**) and (**i**), respectively. (**j**) Western blot analysis of immunoprecipitates of Flag-IRE1α in transfected HEK293T cells, showing reduced ubiquitination of T3A IRE1α and interaction with Hrd1. (a), (b) and (j) are representative of 2 independent experiments, while others are representative of 3 independent experiments. (d) and (h), data represent sem of n=3 independent experiments. **, $p<0.01$, ***, $p<0.001$ Student's two-tailed *t* test. Unprocessed original scans of blots are shown in Supplementary Fig. 9.

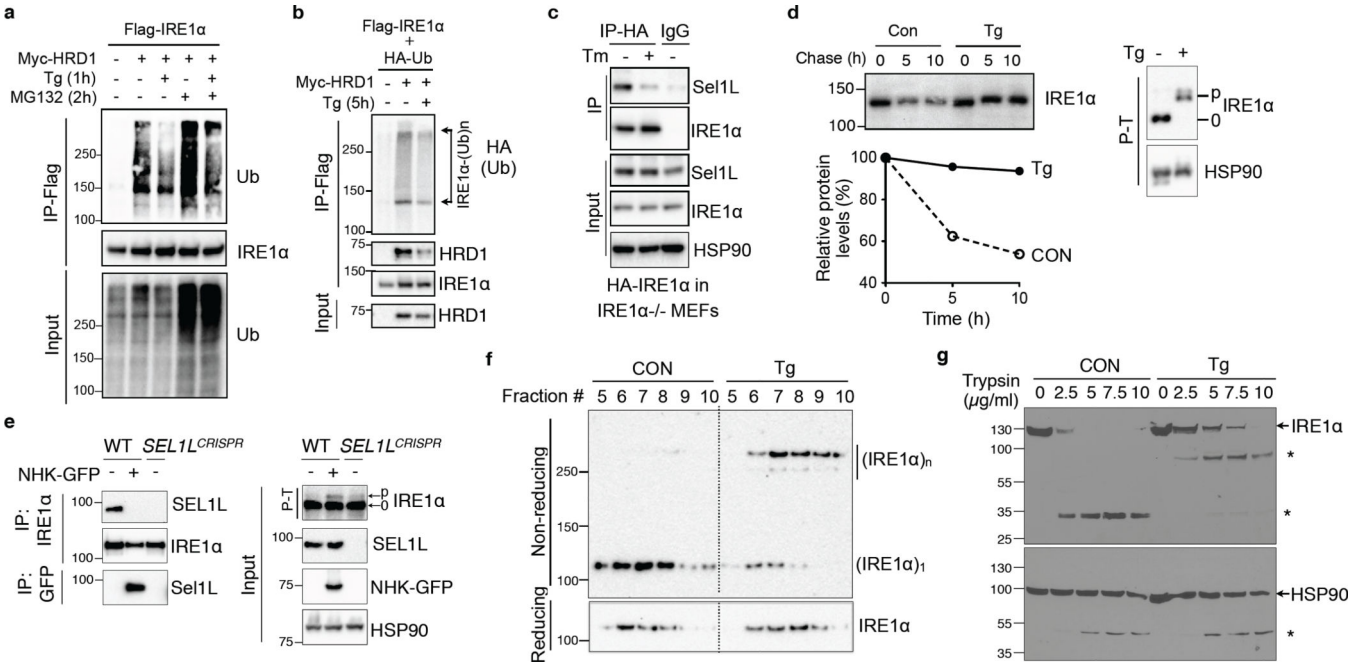

Figure 3. Sel1L-Hrd1-mediated IRE1α degradation is regulated by ER stress

(**a–b**) Western blot analysis of immunoprecipitates of Flag-agarose in transfected HEK293T treated with 200 nM thapsigargin (Tg) and/or 10 μM MG132. (**c**) Western blot analysis of immunoprecipitates of HA-agarose in IRE1α−/− MEFs stably expressing HA-IRE1α. Tm, 2.5 μg/ml tunicamycin for 2 h. (**d**) Pulse-chase analysis of IRE1α decay in HEK293T cells transfected with HA-IRE1α. Cells were treated with 300 nM Tg during the chase. Quantitation shown below. Phos-tag-based (P–T) Western blot analysis on the right indicated strong IRE1α phosphorylation and activation in response to Tg. (**e**) Western blot analysis of immunoprecipitates in WT and SEL1L-deficient (*SEL1L*^{CRISPR}) HEK293T cells transiently transfected with NHK-GFP. (**f**) Sucrose gradient followed by Western blot analyses under non-reducing and reducing conditions in mock- or Tg-treated MEFs. (**g**) Limited proteolysis digestion of IRE1α in lysates from HEK293T cells treated with or without 100 nM Tg for 3 h, showing conformational change of IRE1α. *, degradation intermediates. Representative data from two independent experiments shown. Unprocessed original scans of blots are shown in Supplementary Fig. 9.

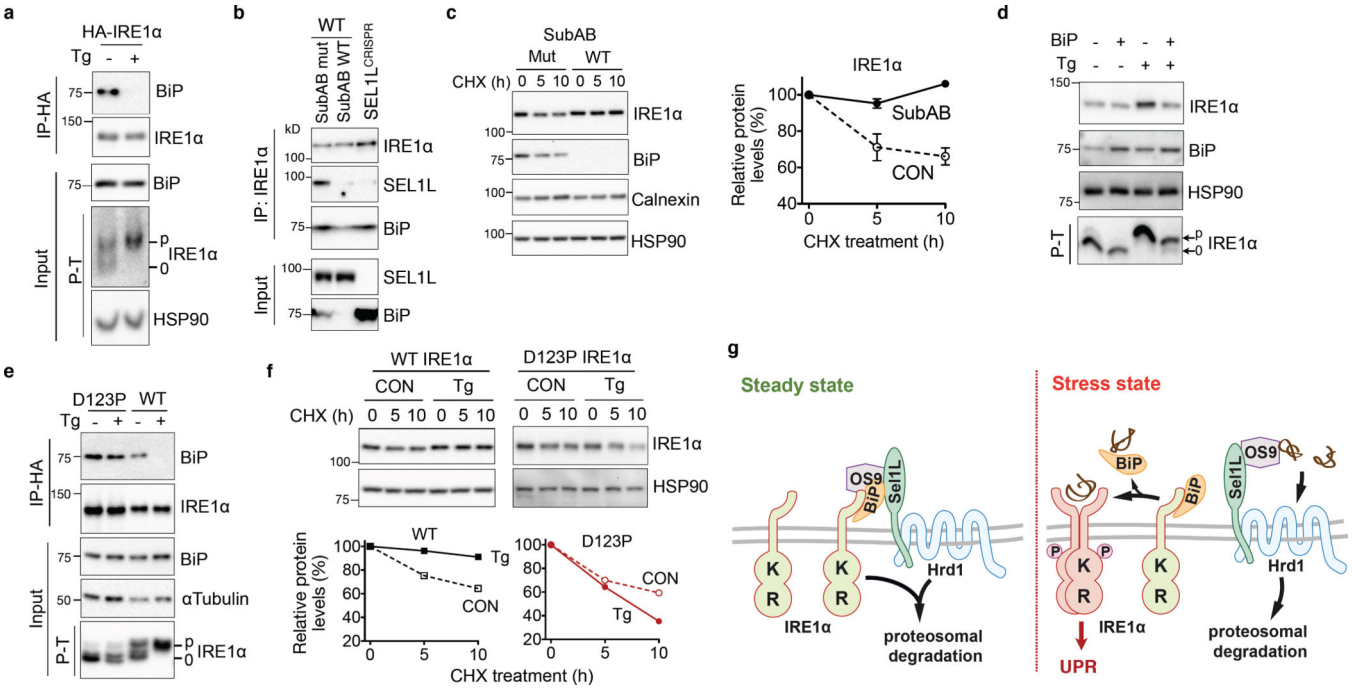

Figure 4. Sel1L-Hrd1-mediated IRE1α degradation requires BiP

(**a**) Western blot analysis of immunoprecipitates in mock- or Tg-treated HEK293T cells expressing HA-IRE1α. (**b**) Western blot analysis of immunoprecipitates in HEK293T cells treated with 1 μg/mL WT SubAB or mutant $SubA_{A272}B$ (mut) for 1 h, showing that BiP links IRE1α to Sel1L. (**c**) Western blot analysis of IRE1α in MEFs pre-treated with 1 μg/mL WT SubAB or mutant $SubA_{A272}B$ (mut) for 1 h followed by cycloheximide (CHX) for the indicated time with quantitation shown on the right. Error bars represent sem, n=3 independent experiments. (**d**) Western blot analysis of IRE1α in MEFs with ectopic expression of BiP, with or without Tg treatment. (**e**) Western blot analysis of immunoprecipitates in IRE1α−/− MEFs stably expressing either WT or D123P HA-IRE1α, with or without Tg treatment. (**f**) Western blot analysis of IRE1α in IRE1α−/− MEFs stably expressing either WT or D123P HA-IRE1α, pre-treated with 300 nM Tg for 2 h followed by CHX treament. Quantitation shown below. (a) and (c) are representative of 3 independent experiments, while others are representative of 2 independent experiments. P–T, phos-tag-based Western blot to visualize IRE1α phosphorylation. (**g**) Model for ERAD-mediated IRE1α degradation under basal and stress conditions. Unprocessed original scans of blots are shown in Supplementary Fig. 9.

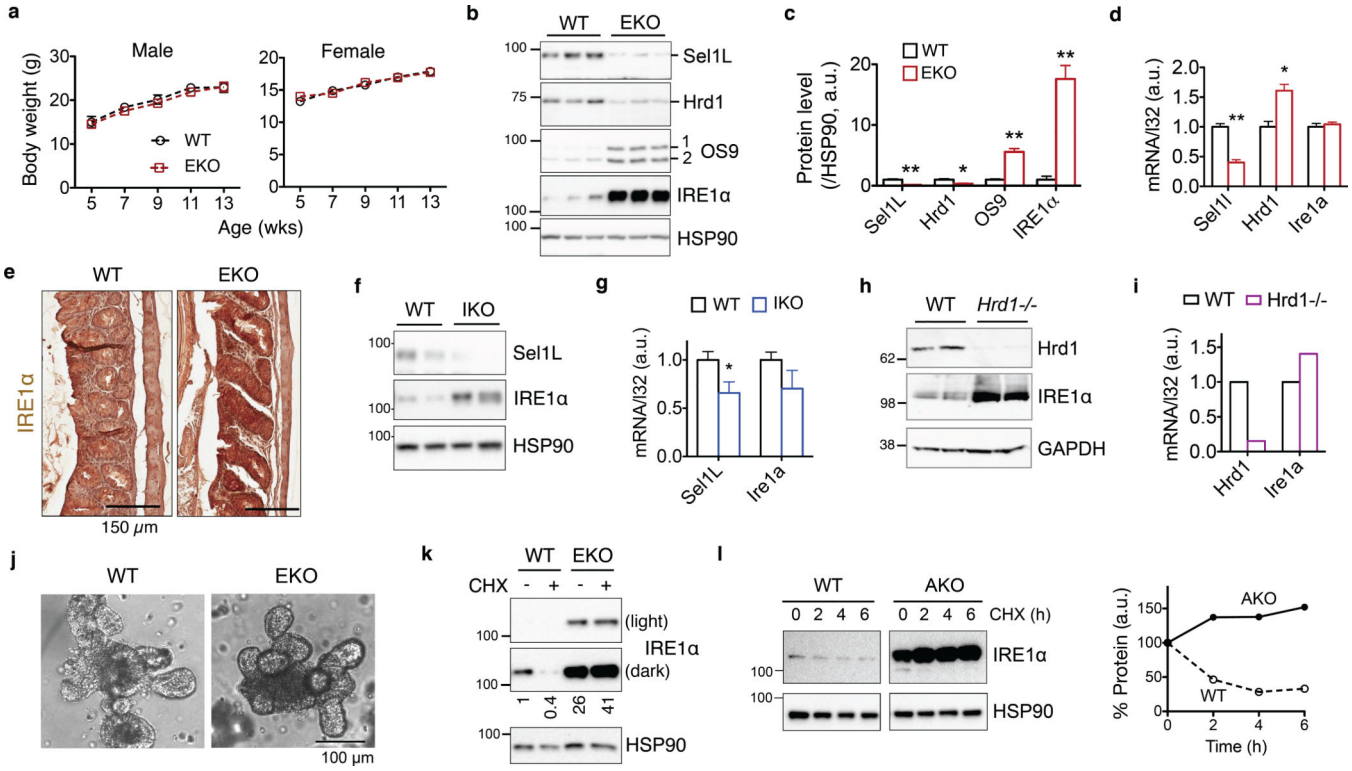

Figure 5. IRE1α is an endogenous Sel1L-Hrd1 substrate in vivo

(a) Growth curve of adult WT and *Sel1L*$^{\Delta IEC}$ (EKO) mice (showing the mean for 5 mice of each genotype at each time point). **(b–c)** Western blot analysis of IRE1α and Sel1L-Hrd1 ERAD protein levels in isolated colonic epithelium of WT and EKO mice, with quantitation shown in **(c)**. Each lane represents an independent sample. HSP90, a loading control. Error bars represent sem, n=3 mice of each genotype. **(d)** Q-PCR analysis of *Sel1l*, *Hrd1* and *Ire1α* mRNA levels in the gut. Error bars represent sem, n=3 mice of each genotype. **(e)** Immunohistochemical staining of IRE1α in colon. Representative images of 3 mice studied. **(f–g)** Western blot and Q-PCR analyses of Sel1L and IRE1α in the gut of *Sel1Lf/f;ERCre−* (WT) and *Sel1Lf/f;ERCre+* (IKO) mice 13 days post-tamoxifen injection. Error bars represent sem, n=5 mice of each genotype (only two shown for Western blots). **(h–i)** Western blot and Q-PCR analyses of Hrd1 and IRE1α in the gut of *Hrd1+/+;ERCre+* (WT) and *Hrd1f/f;ERCre+* (*Hrd1−/−*) mice 10 days post-tamoxifen injection. n=2 mice of each genotype. **(j)** Representative images of primary crypt organoids in culture. **(k)** Western blot analysis of primary intestinal crypt organoids treated with 25 μg/ml cycloheximide (CHX) for 2 h, with quantitation shown below the blot. **(l)** Western blot analysis of IRE1α in primary adipocytes from WT or adipocyte-specific *Sel1L*-deficient (AKO) mice treated with 50 μg/ml cycloheximide (CHX) for the indicated time, with quantitation shown on the right. Representative data from two independent repeats shown. *, $p<0.05$; **, $p<0.01$ by Student's two-tailed *t* test. Unprocessed original scans of blots are shown in Supplementary Fig. 9.

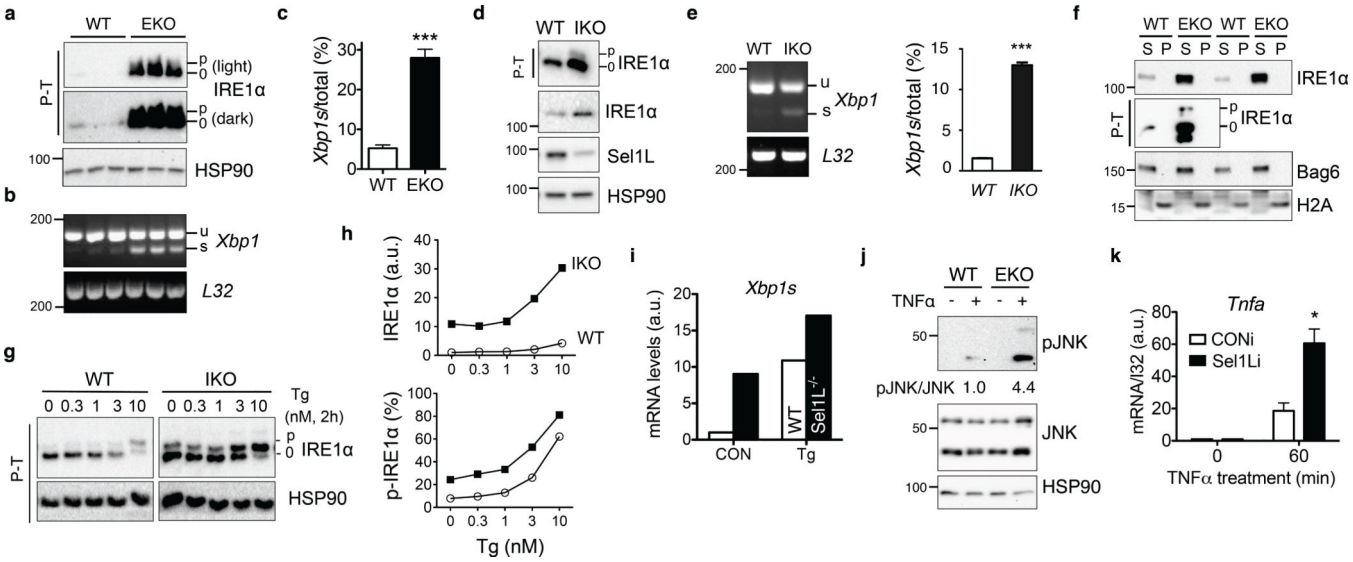

Figure 6. Consequences of Sel1L-Hrd1 ERAD deficiency on IRE1α activation and inflammation

(a) Phos-tag-based (P-T) Western blot analysis of IRE1α phosphorylation in isolated colonic epithelium of WT and *Sel1L*$^{\Delta IEC}$ (EKO) mice. N=3 mice of each genotype. **(b–c)** RT-PCR analysis of *Xbp1* mRNA splicing, with quantitation shown in **(c)**. Error bars represent sem, n=3 mice of each genotype. **(d–e)** Western blot and RT-PCR analyses of IRE1α activation in WT and IKO MEFs, with quantitation of spliced *Xbp1* shown in **(e)**. Error bars represent sem, n=3 independent experiments. **(f)** Western blot analysis of IRE1α in the NP-40 soluble (S) and insoluble (P) fractions of the colon using lysis buffer containing 0.5% NP-40. The distribution of Bag6 and H2A marks the soluble and insoluble pellet fractions, respectively. **(g–h)** Western blot analysis of IRE1α activation in WT and IKO MEFs treated with thapsigargin (Tg) at the indicated concentration for 2 h, with quantitation of total p-IRE1α and percent of p-IRE1α shown in **(h)**. In **(g)**, data was derived from the same blot at the same exposure, with irrelevant lanes in the middle cut off. **(i)** Q-PCR analysis of mRNA levels of *Xbp1s* in WT and *Sel1L*-deficient primary adipocytes that were either mock (CON) or treated with 150 nM Tg for 3 h. n=2 mice per genotype. **(j–k)** *Sel1L* deficiency enhances inflammatory tone of enterocytes. **(j)** Primary crypt organoids were treated with 50 ng/ml TNFα for 20 min and analyzed for JNK phosphorylation. Quantitation of the average of n=2 mice of each genotype shown below the blot. (**k**) m-IC$_{cl2}$enterocytes stably expressing either control (CONi) or *Sel1L* knockdown (*Sel1Li*) were treated with 50 ng/mL murine TNFα for 60 min and analyzed for *Tnfa* gene expression. Error bars represent sem, n=3 independent experiments. (a–e) and (k) are representative of 3 independent experiments, while others are representative of 2 independent experiments. *, $p<0.05$; ***, $p<0.001$ by Student's two-tailed *t* test. Unprocessed original scans of blots are shown in Supplementary Fig. 9.

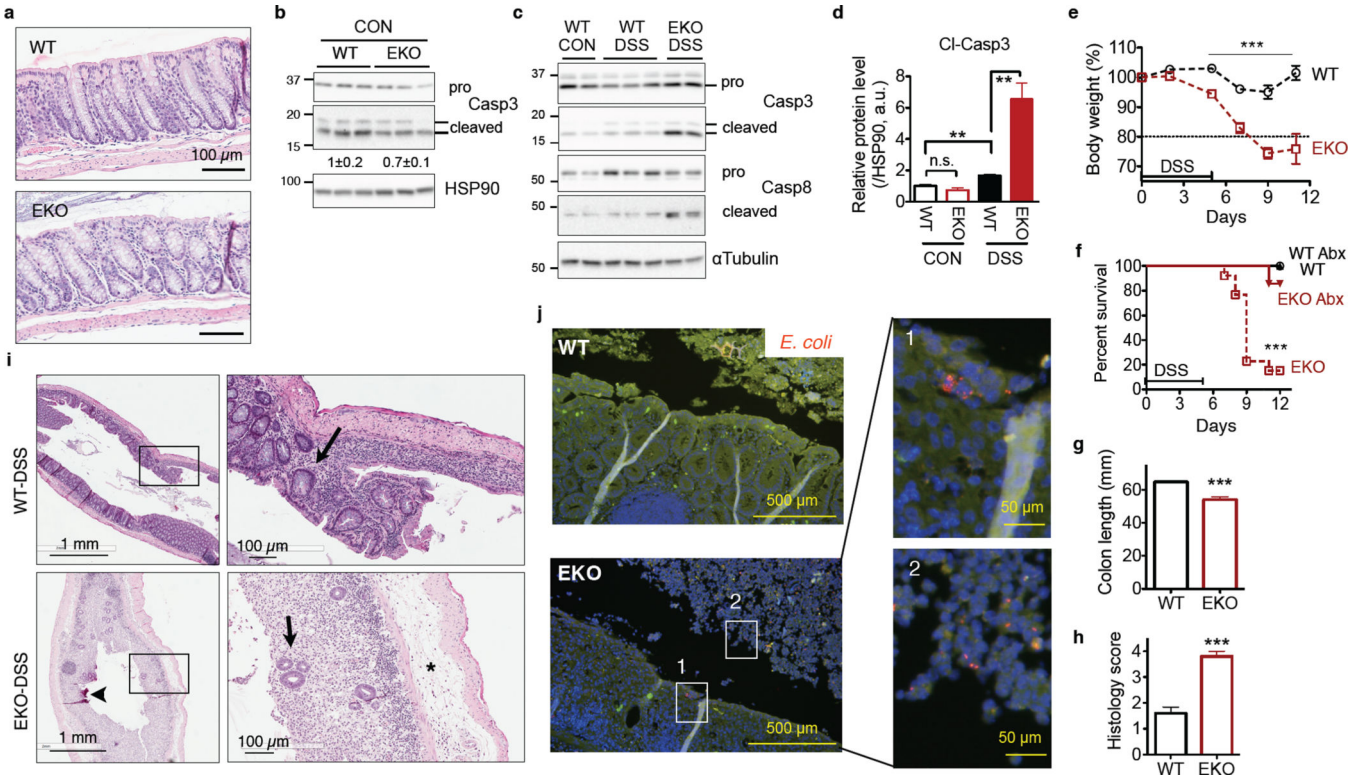

Figure 7. *Sel1L*$^{\Delta IEC}$ (EKO) mice are susceptible to experimental colitis

(**a**) Gross colon morphology of 14-wk-old WT and *Sel1L*$^{\Delta IEC}$ mice. Representative images of 5 mice studied. (**b–j**)12-wk-old mice were treated with 3% DSS for 5 days followed by fresh water. (**b–c**) Western blot analysis of caspase-3 or -8 cleavage in colon epithelium before or on day 7 after DSS-treatment. Quantitation is shown in (**d**). CON, before DSS treatment. Error bars represent sem, n=3 mice of each genotype. (**e**) Body weight change. Error bars represent sem from n=11 mice of each genotype pooled from two independent experiments. (**f**) Survival curve of DSS-treated mice with or without antibiotics (Abx). ***, p<0.001 comparing EKO to the other cohorts by the log-rank Mantel–Cox test. Combined data from n=7 (with Abx) and 13 mice (without Abx) each genotype. (**g**) Colon length on day 9. Error bars represent sem from n=6 WT and n=5 EKO mice. (**h**) Inflammatory score of colon on day 9 as a blind study. 0, none; 1, low; 2, moderate; 3, high; 4, maximal. Error bars represent sem from n=11 mice of each genotype. (**i**) H&E images of colon on day 9 showing epithelial ulceration (arrow heads), severe edema (asterisks), and regenerative crypts (arrows). Representative images of 5 mice studied. (**j**) FISH staining showing the presence of *E. coli* (red), rarely found in WT mice, in the colonic mucosa of DSS-treated mice on day 9. Green, non-specific signal; blue, DAPI-stained nucleus. Panels 1 and 2 show invasive *E. coli* in colonic mucosa and sloughed-off epithelia, respectively, of EKO mice. Representative images of 3 mice studied. n.s., not significant; **, p<0.01; ***, p<0.001 by Student's two-tailed t test unless otherwise indicated. Unprocessed original scans of blots are shown in Supplementary Fig. 9.

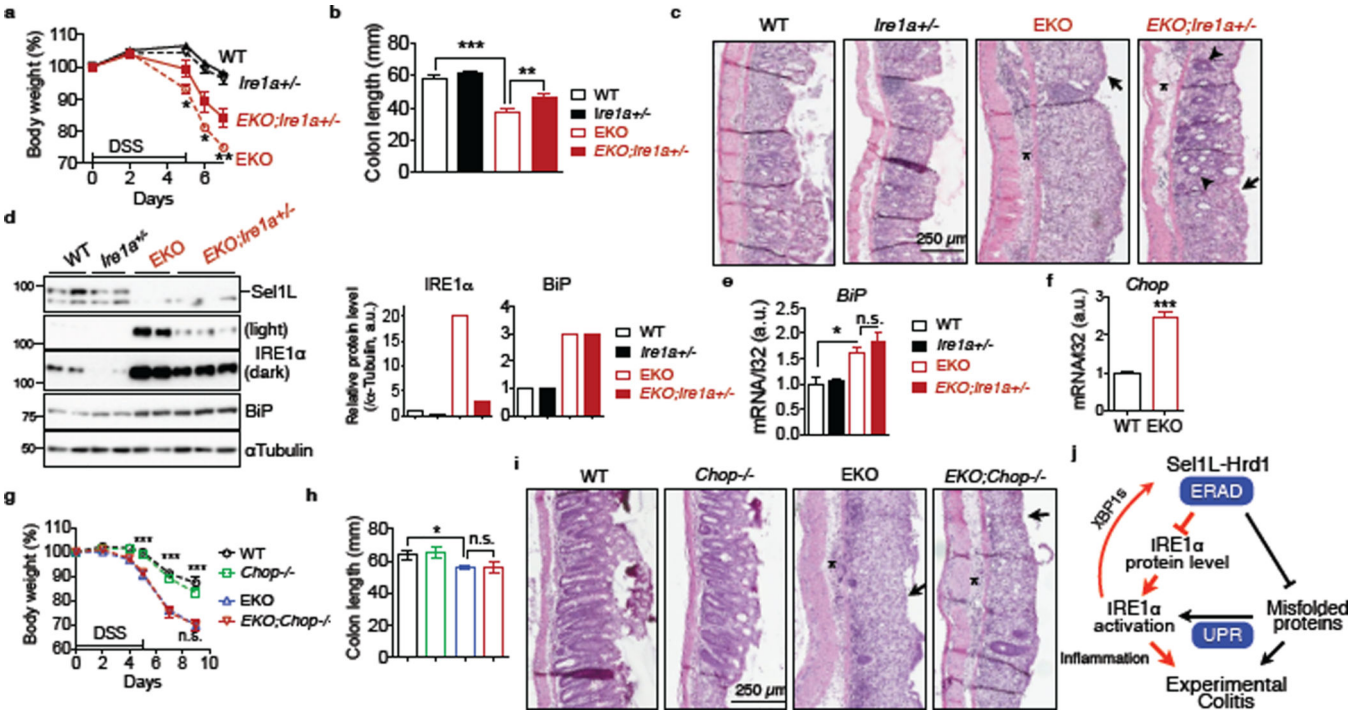

Figure 8. IRE1α protein accumulation is critical for the pathogenesis of colitis in *Sel1L*$^{\Delta IEC}$ (EKO) mice

(**a–c**) 7-week-old littermates were treated with 3% DSS for 5 days followed by fresh water: (**a**) body weight change. *, $p<0.05$; **, $p<0.01$ comparing EKO to EKO;*Ire1a+/−* by Student's *t* test. (**b**) Colon length on day 7. (a-b), error bars represent sem from n=6 mice of each genotype pooled from three independent experiments. (**c**) Representative H&E images of colon on day 7 showing epithelial ulceration (arrows), severe edema (asterisks), and regenerative crypts (arrow heads). Representative images of 6 mice studied. (**d**) Western blot analysis of IRE1α and Sel1L protein levels in the gut, with quantitation shown on the right (n=3 mice for EKO;*Ire1a+/−* and n=2 for the rest). Each lane represents an independent sample. αTubulin, a loading control. Unprocessed original scans of blots are shown in Supplementary Fig. 9. (**e**) Q-PCR analysis of *BiP* mRNA levels in the gut. Error bars represent sem, n=3 mice of each genotype. (**f**) Q-PCR analysis of *Chop* mRNA levels in isolated colon epithelium of WT and *Sel1L*$^{\Delta IEC}$ mice. Error bars represent sem, n=3 mice of each genotype. (**g–i**) The experiments and data presentation are the same as those shown above in (a-c), with the exception that *EKO;Chop−/−* and their control cohorts were characterized. Error bars represent sem from n=6 mice of each genotype pooled from two independent experiments. n.s., not significant. *, $p<0.05$; **, $p<0.01$; ***, $p<0.001$ by Student's two-tailed *t* test. (**j**) Our model: Sel1L-Hrd1 ERAD degrades IRE1α protein, thereby restraining IRE1α activation and signaling. Subsequently, IRE1α signaling modulates inflammation and the pathogenesis of experimental colitis. The finding reported in this study is shown in red.